nature reviews methods primers

https://doi.org/10.1038/s43586-024-00373-9

Primer

Check for updates

Perovskite solar cells

Jiye Han[1,10], Keonwoo Park[1,10], Shaun Tan[2,10], Yana Vaynzof[3,4], Jingjing Xue[5,6], Eric Wei-Guang Diau[7,8], Moungi G. Bawendi[2] ✉, Jin-Wook Lee[1,9] ✉ & Il Jeon[1] ✉

Abstract

Photovoltaic technologies have emerged as crucial solutions to the global energy crisis and climate change challenges. Although silicon-based solar cells have long dominated the market, metal halide perovskite solar cells (PSCs) have rapidly advanced as a promising alternative. Despite their relatively short history, PSCs are progressing at an unprecedented rate, driven by global research efforts that capitalize on their unique advantages. These innovative cells offer lower manufacturing costs, simpler fabrication processes and greater mechanical flexibility compared with traditional silicon cells. Remarkably, their power conversion efficiency has recently surpassed 26%, approaching that of silicon cells. This Primer outlines the diverse fabrication methods for high-performance PSCs, focusing on three key components: the photoactive layer, charge-transporting layers and electrodes. The photoactive layer, typically made of ABX_3 perovskite materials, is crucial for light absorption and forms the cornerstone of device functionality. Charge-transporting layers, specifically the electron and hole transport layers, facilitate efficient charge movement and mitigate recombination losses, enhancing overall cell performance. Electrodes, traditionally formed by pure metals or metal oxides, complete the cell structure and govern additional functionalities, such as mechanical flexibility and cell transparency. This Primer concludes by examining current limitations and offers insights into the future prospects of PSCs.

Sections

[1]Department of Nano Engineering, Department of Nano Science and Technology, SKKU Advanced Institute of Nanotechnology (SAINT), Sungkyunkwan University (SKKU), Suwon, Gyeonggi-do, Republic of Korea. [2]Department of Chemistry, Massachusetts Institute of Technology (MIT), Cambridge, MA, USA. [3]Chair for Emerging Electronic Technologies, Technische Universität Dresden, Dresden, Germany. [4]Leibniz Institute for Solid State and Materials Research Dresden, Dresden, Germany. [5]State Key Laboratory of Silicon and Advanced Semiconductor Materials, School of Materials Science and Engineering, Zhejiang University, Hangzhou, China. [6]Shangyu Institute of Semiconductor Materials, Shaoxing, China. [7]Department of Applied Chemistry and Institute of Molecular Science, National Yang Ming Chiao Tung University, Hsinchu, Taiwan. [8]Center for Emergent Functional Matter Science, National Yang Ming Chiao Tung University, Hsinchu, Taiwan. [9]SKKU Institute of Energy Science & Technology (SIEST), Sungkyunkwan University (SKKU), Suwon, Gyeonggi-do, Republic of Korea. [10]These authors contributed equally: Jiye Han, Keonwoo Park, Shaun Tan. ✉e-mail: mgb@mit.edu; jw.lee@skku.edu; il.jeon@spc.oxon.org

Introduction

In response to the pressing challenges of climate change and the energy crisis, the solar industry has experienced a resurgence, marked by a notable increase in demand for renewable energy sources. Perovskite-based solar cells (PSCs) have emerged as the leading next-generation photovoltaics, with formidable power conversion efficiency (PCE), solution processability and mechanical flexibility, surpassing conventional silicon-based counterparts. These properties align with the requirements for cutting-edge photovoltaic systems. PSC technology has developed rapidly since the seminal liquid electrolyte-based prototype reported in 2009 (ref. 1). A noteworthy advance was the transition from liquid electrolytes — with a PCE of 3.81% — to solid-state counterparts, based on 2,2′,7,7′-tetrakis[*N*,*N*-di(4-methoxyphenyl)amino]-9,9′-spirobifluorene (spiro-MeOTAD), which have PCEs of 9.7%[2] and 10.9%[3]. This breakthrough led to further PCE improvements, enhanced device longevity and the addition of features, such as flexibility and semi-transparency. Presently, the highest certified PCE for PSCs is 26.7%, accredited by the National Renewable Energy Laboratory[4].

Innovations in fabrication and analysis have driven progress in PSCs. At the core of PSCs is the metal halide perovskite photoactive thin film. This photoactive layer, also known as the active layer, is the core component for converting light into electricity. When sunlight strikes the perovskite, it generates electron–hole pairs. The charge-selective layers, also known as the charge transport layer, efficiently collect charges to create an electric field. As electrons flow through an external circuit and recombine with holes, they produce an electric current. Understanding the perovskite active layer is crucial, as its exceptional light absorption and charge transport properties are key to solar cell performance. The perovskite photoactive thin film has the chemical composition ABX_3, in which A is an organic or inorganic cation, B is a metal cation and X is a halide anion (Fig. 1a). PSCs can be broadly categorized as organic–inorganic hybrid or fully inorganic depending on the choice of A. The material and stoichiometric ratio of A, B and X components are crucial, as they determine the absorption characteristics and film quality, which translates to PCE and device stability. The size of each component affects the tolerance factor of the perovskite structure, which influences phase formation, overall stability and film bandgap. By understanding the relationship between chemical composition and PSC performance, advances can be gained through material, process and device engineering. This includes incorporating 2D perovskites, solvent[5,6] and additive engineering[7–10], composition adjustment[11,12], morphology control[5,13] and interface modification[14–16].

PSCs are technologically comprehensive devices, and their overall performance is determined not only by the perovskite active layer, but also by the adjacent charge-selective layers and electrodes. Methods of fabricating (Table 1) and evaluating these layers have an equally important role in advancing PSC technology. Normative PSCs share a common architecture of a photoactive layer sandwiched between a pair of charge-selective layers and electrodes. There are two main structural configurations: normal (or conventional) and inverted types, denoted as n–i–p and p–i–n, respectively (Fig. 1a). These abbreviations represent the order of the layers in the cell, in which n is the electron transport layer (ETL), i is the intrinsic perovskite absorber layer and p is the hole transport layer (HTL). In the n–i–p (normal) structure, light enters the ETL, passes through the perovskite layer and finally reaches the HTL. Conversely, in the p–i–n (inverted) structure, light enters the HTL, passes through the perovskite layer and finally reaches the ETL. The choice between normal and inverted structures influences various aspects of PSC performance, including stability, hysteresis and efficiency. Each structure has unique merits and drawbacks in design and function. The two PSC types have different energy levels and are sensitive to the bandgaps and Fermi levels of the component layers (Fig. 1b). The bandgap of perovskite materials can be tuned by composition engineering (Fig. 1c,d), with all A, B and X sites having an influence. For instance, the bandgaps for $MAPbI_3$, formamidinium lead iodide ($FAPbI_3$) and $CsPbI_3$ perovskites are about 1.59, 1.51 and 1.72 eV, respectively[17]. The bandgap increases as the ionic radius of the A-site decreases, owing to modulation of the Pb–I bond from size effects in the A-site cations[18]. X-site regulation is also a widely used approach for regulating perovskite bandgap[19,20]. The nonlinear trend in bandgap variation arises from the energy disparity between the s/p atomic orbitals of tin, which contribute to the band edges of the alloy[19]. In tin-based perovskites, the coupling between the conduction and valence band edges is weaker than in lead-based counterparts as tin has less strongly bonded atomic orbitals. This suggests that the valence band maximum derived from tin and the conduction band minimum originating from lead determine the alloy bandgap range.

This Primer introduces the diverse fabrication methods and techniques used to craft PSCs. A wide range of perovskite types, charge-selective layers and electrodes are discussed, focusing on the most effective strategies for achieving high performance. For the active layer, common deposition methods include spin coating, slot-die coating and thermal evaporation. Similarly, for the charge-selective layer, spin coating, spray coating, thermal evaporation and sputtering are typically used. Electrodes are often fabricated by sputtering, thermal evaporation, atomic layer deposition (ALD), direct lamination and inkjet printing. The Experimentation section discusses the active layer and charge-selective layer from wet (solution) and dry perspectives, whereas electrodes are viewed from the transparent bottom and counter top standpoints. For the active layer, the four mainstream regimes — traditional organic–inorganic, quantum dot, lead free and double perovskites — are discussed in depth. The Results section explores evaluation methods for PSC performance and analysis techniques for each component. The Applications section introduces realistically viable commercial markets based on PSC functionalities. The Limitations and optimizations section looks at critical bottlenecks and how to overcome them. Finally, the Outlook section provides a future-focused perspective of PSCs.

Experimentation

Active layer: lead perovskites from solution

Record-breaking efficiencies in PSCs were achieved with compositions based on $FAPbI_3$ as the photoactive layer[21–23]. Pure $FAPbI_3$ offers a close-to-ideal narrow bandgap (~1.48 eV) and better thermal stability compared with other compositions. However, it suffers from phase instability, undergoing an undesirable transformation from the photoactive, black, perovskite α-phase to the photo-inactive, yellow, non-perovskite δ-phase at room temperature (RT)[24,25] (Fig. 2a). The α-phase of $FAPbI_3$ has a higher formation enthalpy because the large FA^+ cation causes a high tolerance factor ($t \approx 0.99$) and intrinsic strain in the $[PbI_6]^{-4}$ octahedral framework, increasing the lattice energy and formation enthalpy[24–26]. At lower temperatures, the rotational freedom and dynamic motion of FA^+ cations are restricted, reducing the entropy contribution to the Gibbs free energy[27–29]. Consequently, cubic α-$FAPbI_3$ is favoured at higher temperatures (>390 K) owing to higher entropy[26,30]. The combination of lower entropy and higher enthalpy makes α-$FAPbI_3$ less stable at RT than hexagonal δ-$FAPbI_3$, leading to a

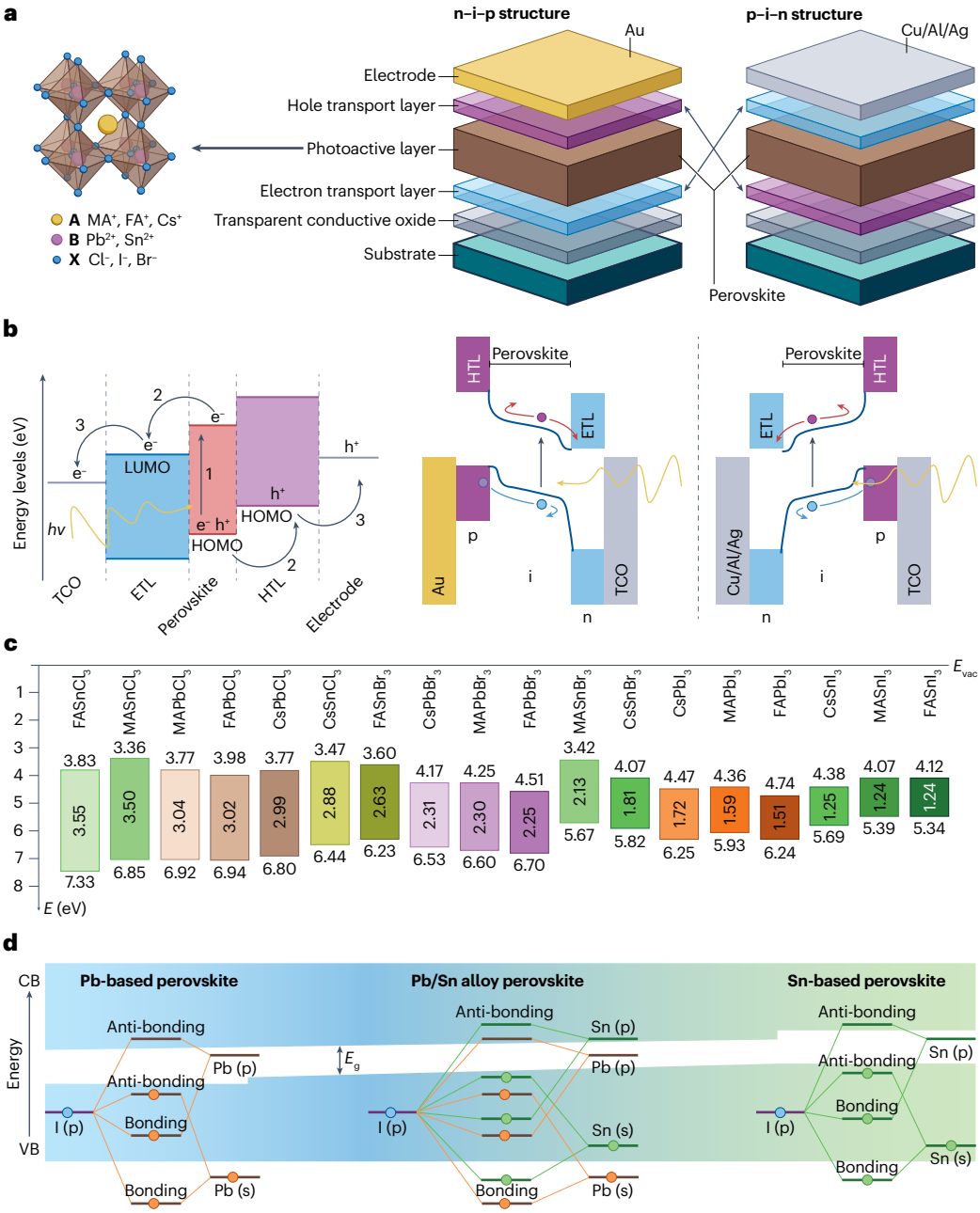

Fig. 1 | Schematic diagram illustrating the operating principles of perovskite solar cells. a, Schematic diagram of the base perovskite crystal and two perovskite solar cell (PSC) device structures (p–i–n and n–i–p). **b**, Band diagram and operation principle of PSCs. **c**, Schematic energy level diagrams of various metal halide perovskites. **d**, Illustration of the bandgap origin of band bending in Pb/Sn double perovskite. Shaded areas denote the valence and conduction bands, whereas thick lines represent the molecular orbital framework, highlighting the formation of electronic bands within the alloy. CB, conduction band; ETL, electron transport layer; FA, formamidinium; HOMO, highest occupied molecular orbital; HTL, hole transport layer; LUMO, lowest unoccupied molecular orbital; MA, methylammonium; TCO, transparent conducting oxide; VB, valence band.

spontaneous transformation to the δ-phase. This phase instability is a challenge for practical application of $FAPbI_3$-based PSCs. To address these challenges, several strategies were developed to promote formation and stabilization of the α-$FAPbI_3$ phase, without compromising its intrinsic properties (Fig. 2b). The main approaches include compositional engineering, solvent engineering and volatile additives, which focus on forming a stable intermediate α-phase during fabrication, while preventing conversion back to the δ-phase after film formation (Fig. 2b,c).

Compositional engineering stabilizes the α-phase by modifying its chemical composition. Often, multiple cation combinations are used, incorporating a specific ratio of bromide (Br^-) to enhance stability. For

Table 1 | Perovskite solar cell fabrication methods and their features

Material type	Fabrication method	Advantages	Disadvantages
Active layer			
$APbX_3$	One-step spin coating (S)	Fast and facile process Low cost	Limited to a small area Smooth morphology required Low reproducibility owing to antisolvent timing
	Two-step spin coating (S)	Facile process High reproducibility Low cost	Incomplete perovskite phase conversion Difficulty with chemical composition control
	D-bar coating (S)	Uniform film thickness Scalable large area coating	Difficulties in crystallization control owing to slow solvent evaporation
	Slot-die coating (S)	Suitable for roll-to-roll process Wastes less solution	Non-uniform film thickness owing to edge effect Rough morphology
	Co-evaporation (D)	High uniformity Smooth morphology Scalable and industrially viable	Complexity in precursor ratio control Sophisticated equipment needed Requires precise deposition monitor
	Sequential evaporation (D)	Precise control over stoichiometry and thickness of each layer Useful for complex compositions	Difficult to induce solid–vapour reaction Complex deposition rate control
	Hybrid deposition (S/D)	Advantages of solution and evaporation approaches	Complex fabrication process Disadvantages of solution and evaporation approaches
Perovskite quantum dots	Sequential layer-by-layer deposition (S)	Good control over film thickness Good film coverage	Complex, multistep process involving multilayer deposition and ligand washing
Tin-based perovskites	One-step spin coating (S)	Fast and facile process Low cost	Inconsistent crystallization Tin oxidation
	Two-step spin coating (S)	More controlled crystallization Good film coverage	Complex and long process Potential for incomplete crystallization
	Sequential deposition (S)	Reduces oxidation Excellent film coverage	Highly complex and longer process More solution waste
Charge-selective layer			
Metal oxides	Spin coating (S)	Low cost Easier scale-up to large areas Compatible with flexible substrates	Requires post-treatment, usually thermal Cannot be applied on perovskite layer
	Sputtering (D)	High film quality Precise control over film thickness and composition	High cost Bombardment damage
	ALD (S/D)		High cost Chemical damage Requires post-treatment, usually thermal
Organic materials	Spin coating (S)	Fast and facile Low cost	Certain solvents may damage perovskite layer
	Thermal evaporation (D)	High-quality layer Fine thickness control	High cost Difficult to control thickness
Electrode layers			
Metals	Spin coating metal nanowires (S)	Fast and facile	Induces ion migration Bottom electrode only Rough morphology Causes glare
	Thermal evaporation (D)	Highest conductivity	Induces ion migration High cost and slow process Causes glare
Metal oxides	Sputtering (D)	Good conductivity and transparency	Mechanically inflexible Rare-earth metals High cost

Table 1 (continued) | Perovskite solar cell fabrication methods and their features

Material type	Fabrication method	Advantages	Disadvantages
Electrode layers (continued)			
Carbon (graphene)	Spin coating of reduced graphene oxide (S)	Facile and low cost Mechanically flexible	Low conductivity Requires a reduction step Bottom electrode only
	Wet transfer (S/D)	Highly transparent, especially in the infrared region Earth abundant Mechanically flexible	Slow process and low reproducibility Residual impurity Bottom electrode only
	Dry transfer (D)		Slow process and low reproducibility Requires adhesive removal treatment Bottom electrode only
Carbon (carbon paste)	Lamination (S/D)	Earth abundant Excellent device stability Mechanically flexible Low cost	Non-transparent Top electrode only Requires high temperature annealing (>500 °C)>μm thickness
Carbon (carbon nanotube)	Spin coating (S)	Low cost Earth abundant Mechanically flexible	Limited to bottom electrode owing to solvent damage Surfactants need to be removed
	Lamination (D)	High conductivity and transparency Earth abundant Applicable to both top and bottom electrodes	Chemical doping needed for better conductivity Rough morphology

ALD, atomic layer deposition; (D), dry method; (S), solution method; (S/D), solution and dry method.

instance, $FA_{1-x}MA_xPb(I_{1-y}Br_y)_3$ (refs. 31–34) and $FA_{1-(x+y)}MA_xCs_y(I_{1-(y+x)}Br_{y+x})$ (refs. 35–40) were developed to stabilize the α-phase of $FAPbI_3$. Replacing FA^+ with smaller cations, such as caesium (Cs^+) or methylammonium (MA^+), reduces the tolerance factor and alleviates lattice strain. This substitution lowers the formation enthalpy and enhances overall stability, as illustrated in Fig. 3a,b (refs. 41,42). Partial substitution of I^- with Br^-, which has stronger electronegativity, helps to stabilize the α-$FAPbI_3$ lattice[27]. Although these small-radius ions are effective for controlling lattice stress and lowering the formation energy, it is crucial to maintain a delicate balance when incorporating them. Excessive amounts can compromise the advantageous properties of $FAPbI_3$. Potential drawbacks include widening the bandgap, diminished thermal stability and induction of photoinduced phase segregation[43,44].

Using volatile organic halides, such as methylammonium chloride (MACl), in the perovskite precursor solution can stabilize the high-quality α-phase of formamidinium (FA)-based PSCs[21,35–37,45–48] (Fig. 3c). MACl is initially incorporated into the lattice, promoting the formation of an intermediate α-$FAPbI_3$ at RT[21,49]. The volatility of MACl makes it easy to be removed during annealing, leaving highly crystalline, phase-pure α-$FAPbI_3$. Smaller amounts of non-volatile or less volatile organic halides are also used as additives[21,50,51]. Alkylammonium halides or low-dimensional perovskites formed from alkylammonium halides facilitate formation of α-$FAPbI_3$ by regulating surface energy and templating crystal growth[52].

Solvent engineering based on Lewis acid–base adduct formation is crucial for producing high-quality FA-based perovskite films by solution fabrication[53,54] (Fig. 3d). The approach relies on forming intermediate phases through the coordination of perovskite precursors with Lewis base solvent molecules, such as 1-methyl-2-pyrrolidinone (NMP) or dimethyl sulfoxide (DMSO). Solvents with higher donor numbers tend to form stronger coordination bonds with Pb^{2+}, a Lewis acid, stabilizing intermediate phases and enhancing film uniformity and crystallinity[55]. Strong coordination between the Lewis base and Pb^{2+} results in well-defined intermediate phases that effectively control nucleation and crystal growth to produce uniform films with larger grain sizes. Donor numbers and criteria, such as molecular structure, hardness and softness, should also be considered when selecting compatible solvents for desired perovskite compositions[56]. The volatility and evaporation rate of the solvent are crucial, as optimal rates enable controlled crystallization and uniform films. Ensuring solvent compatibility with the perovskite precursor prevents unwanted reactions and phase separations.

One-step spin coating. One-step spin coating rapidly forms a perovskite from a controlled stoichiometric mixture of organometal halides dissolved in polar aprotic solvents. These solvents typically contain binary[53,56] or ternary systems[57,58], such as *N*,*N*-dimethylformamide (DMF), DMSO or NMP. Antisolvent dripping is often used during spin coating (Fig. 4a). The choice of antisolvent is crucial; it must be compatible with the host solvent while not dissolving the perovskite to promote rapid supersaturation and crystallization into a uniform film. Optimization of one-step spin coating focuses on refining nucleation rates, crystal growth kinetics and intermediate phase regulation to produce highly crystalline and stable phase-pure α-$FAPbI_3$. This is frequently accomplished using Lewis acid–base adducts to decelerate nucleation and crystallization, inducing well-oriented, structured and highly crystalline perovskite films. A complementary approach is compositional engineering — primarily with organic ammonium salts, hydrohalic acids and similar agents — to stabilize α-phase nuclei intermediates. The antisolvent method has shown promise; however, it is dependent on operator skill[59,60]. Improper antisolvent application, particularly regarding speed, timing, position and direction, can lead to

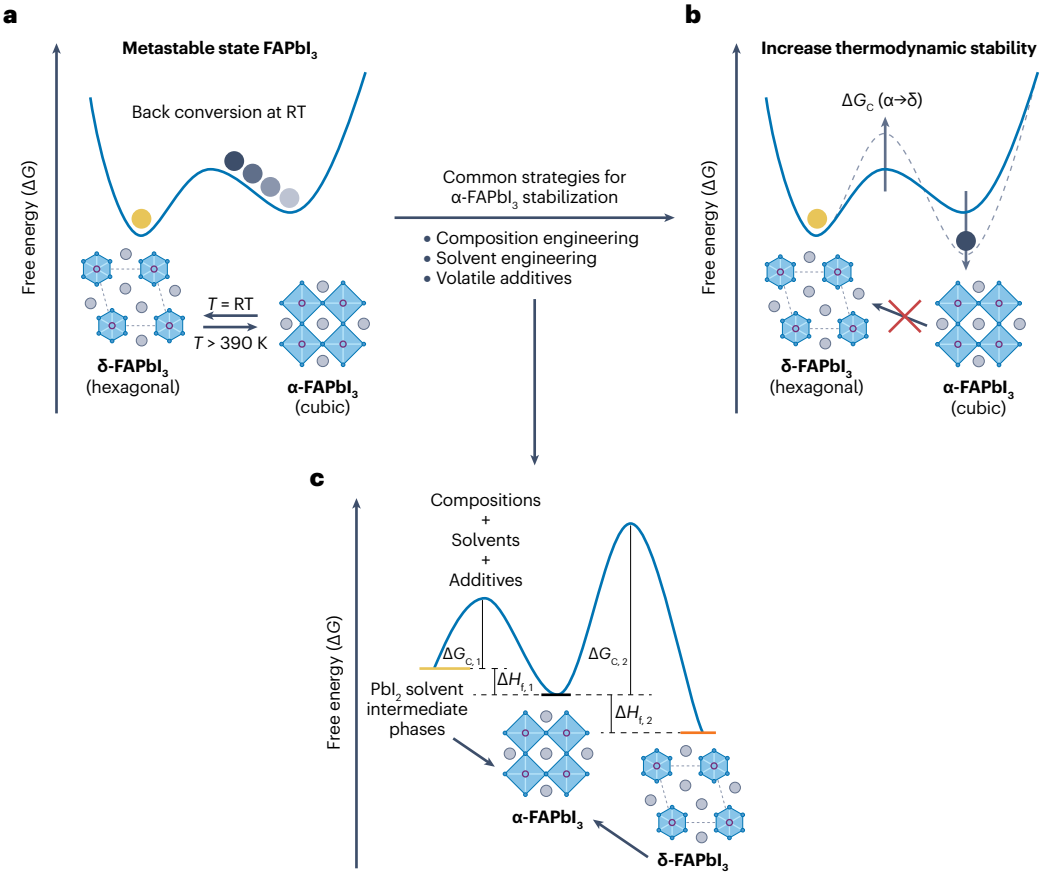

Fig. 2 | Schematic illustration of strategies for α-phase $FAPbI_3$ stabilization. a, Gibbs free energy (ΔG) landscape of metastable formamidinium lead iodide ($FAPbI_3$), illustrating the energy states of α-$FAPbI_3$ and δ-$FAPbI_3$ at room temperature (RT). The α-$FAPbI_3$ has a higher Gibbs free energy compared with the more stable δ-$FAPbI_3$, which causes the α-phase to spontaneously transition to the δ-phase. **b**, Strategies for stabilizing α-phase $FAPbI_3$, focusing on either reducing the ΔG of the α-phase or increasing the energy barrier (ΔG_c) to prevent transition from the α-phase to δ-phase (dashed line). **c**, Differences in Gibbs free energy and enthalpy formation energy during the phase transition from intermediate adducts or δ-$FAPbI_3$ to α-$FAPbI_3$, in which $\Delta H_{f,1}$ represents the formation enthalpy of the cubic $FAPbI_3$ phase from solvent-coordinated intermediate states and $\Delta H_{f,2}$ refers to the formation enthalpy of the cubic $FAPbI_3$ phase from δ-phase $FAPbI_3$.

suboptimal supersaturation of perovskite precursors. Selecting a compatible antisolvent and optimizing process parameters are essential for uniform nucleation and well-coordinated perovskite intermediates.

Two-step spin coating. Two-step spin coating does not use an antisolvent (Fig. 4b). The method begins by separately dissolving lead halide and organic ammonium halide salts. Initially, a PbI_2 precursor is applied to the substrate and spin-coated to form a PbI_2 layer (static spin-coating). Subsequently, an organohalide salt solution, typically dissolved in isopropyl alcohol, is spin-coated onto the PbI_2 layer during the spin-coating process (dynamic spin coating). Two-step spin-coating is marked by a solid–liquid diffusion-driven reaction, which transforms the porous PbI_2 layer into dense perovskite films upon contact with organic ammonium halide salts. The primary challenge lies in controlling crystal growth kinetics and ensuring complete PbI_2 transformation to avoid residual precursors. Similar to the one-step method, modulating crystallization dynamics is crucial to enhance the perovskite layer quality[61]. Intermolecular exchange or introducing seeds in the inorganic layer can catalyse a complete and uniform reaction between precursors, promoting rapid crystal growth[62,63]. Templated growth enables controlled nucleation and growth with a preferred orientation, improving crystallinity and photovoltaic performance. For instance, manipulating seed concentration, controlling heterogeneity by halide engineering or adding Lewis base additives to the inorganic layer gives precise control over crystal growth kinetics. Additives lower the phase conversion activation energy from PbI_2 to perovskite and can act as defect passivation agents. It is essential to remove any residual PbI_2, as PbI_2 photolysis reduces the long-term stability of the film and device. Adding RbCl to PbI_2 can convert inactive PbI_2 to $(PbI_2)_2RbCl$, suppressing non-radiative recombination and enhancing device stability[64].

Post-treatment annealing. Solution-processed perovskite absorbers often require post-treatment thermal annealing to remove residual solvent and ensure the perovskite phase fully crystallizes (Fig. 4c). For $FAPbI_3$ and $CsPbI_3$, thermal annealing is essential to transition from the δ-phase to α-phase[23,25,65]. The annealing temperature and duration must be precisely controlled to prevent the organic component

decomposing to PbI_2, which occurs owing to excessive annealing or incomplete phase conversion. The optimal annealing parameters depend on the perovskite composition. For example, pure $FAPbI_3$ transforms to the cubic phase at 150 °C, whereas $CsPbI_3$ transforms at >300 °C. Mixed-cation compositions with smaller ions — such as MA^+, Cs^+ or Rb^+ — require temperatures below 100 °C to induce the cubic phase transition owing to the relatively small Goldschmidt tolerance factor[34,66,67]. Recent advances include using excess MACl (30–40 mol%) to refine the crystallization and phase energetics of $FAPbI_3$ (ref. 68). Thermal annealing also aims to vapourize volatile MACl, which is a critical step to minimize residual MA^+ and Cl^- and maintain the inherent bandgap of cubic $FAPbI_3$. Because of this, humidity control is important during the annealing process[68,69].

Post-treatment surface passivation. Unlike 3D ABX_3 perovskites, reduced-dimension 2D perovskites have the general formula $L_mA_{n-1}B_nX_{3n+1}$, in which L refers to a bulky organic cation that intercalates between the $[PbX_6]^{4-}$ inorganic layers and n defines the $[PbX_6]^{4-}$ layer number. The bulky organic cation is either monovalent ($m = 2$) or divalent ($m = 1$), and the corresponding 2D perovskite is categorized as the Ruddlesden–Popper ($m = 2$) or Dion–Jacobson ($m = 1$) 2D perovskite phase. Typical bulky organic cations are linear alkylammonium or aromatic ammonium, including butylammonium, octylammonium and phenethylammonium. Although 2D perovskites can function as the absorber layer in solar cells, their efficiency is generally lower than a 3D perovskite counterpart. This disparity stems from the wider bandgap of 2D perovskites and the insulating nature of bulky organic cations, which hinders carrier transport. Two-dimensional perovskites can instead be used as a passivation layer to form 2D/3D perovskite heterojunctions that enhance the efficiency and stability of PSCs[70–72]. Creating 2D/3D perovskite heterojunctions typically involves post-fabrication surface treatment of a 3D perovskite (Fig. 4d). A suitable solvent is needed to dissolve the bulky organic cations[73]. The solvent is then deposited onto the 3D perovskite by solution processing. The choice of solvent is critical. Good solubility of the bulky organic cations is required, without dissolving or damaging the underlying 3D perovskite layer. Polar solvents such as isopropyl alcohol are widely favoured[73]. A subsequent thermal annealing step often promotes reaction between the ligands and lead iodide, forming the 2D perovskite phase. The 2D perovskite layer serves a dual purpose: trap passivation of the 3D perovskite surface and preventing ion migration from corroding the charge transport layer and electrodes. The hydrophobic nature of many bulky organic cations enhances the humidity resistance and environmental stability of the PSC. Designing suitable bulky organic cations can help to ensure effective carrier extraction to the transport layer by considering band alignment[70], ligand–perovskite interaction[74] and deposition of high-quality 2D layers[75].

Scalable processes. Spin-coating-based one-step and two-step fabrication processes are effective for small-area PSCs in laboratory research; however, they are limited for scalable production and commercialization. The challenge is to achieve uniform and highly crystalline perovskite layers with optimal composition and interfacial contacts. To address this, blade coating (D-bar), slot-die, inkjet and spray coating were developed[76–81] (Fig. 4e–g). Although scale-up may require methodology changes, the core principles of modulating crystallization to ensure high crystallinity and uniformity; low defect density and large grain size remain the same. The choice of solvent, which is crucial in any coating technique, influences film formation. Scalable fabrication often uses an antisolvent-free approach, depending on the solvent properties such as boiling point and viscosity. To form dense nuclei and uniform films, it is essential to rapidly remove solvent and control both nucleation and crystallization. Highly volatile solvents can cause crystallization to occur too fast at low temperatures, leading to subpar crystallinity and small grains. To circumvent this, crystallization can be controlled by focusing on solid–liquid interactions and intermediate solvent-complex phase strategies. Slot-die and D-bar coating are particular advantageous for solution-based process scalability.

D-bar coating uses a cylindrical bar to distribute a precursor solution, enabling precise control over film thickness by adjusting the precursor solution volume, coating speed and using an assisted air knife (argon or nitrogen) (Fig. 4e). Blade coating, which is similar to D-bar, uses a different knife-shaped coater rather than a cylindrical blade (Fig. 4f). Scaling up blade coating involves understanding fluid dynamics, increasing deposition speeds and optimizing drying conditions. A critical challenge is to ensure uniform film quality and to avoid defects, such as poor interfacial contacts and perovskite island formation during drying. Surfactants are particularly important for scalable formation of homogeneous films. Perovskite solutions with surfactants produce higher-quality films with improved PCE compared with surfactant-free solutions[82–84]. During drying, microscale fluid flows cause solvent evaporation, which increases the surface tension, resulting in perovskite island formation. Surfactants mitigate this tension and prevent islands by inducing Marangoni flow driven by surface tension gradients.

A slot-die coater contains a slot-die head, or lip, which includes upstream and downstream dies (Fig. 4g). Defect-free films require a stable coating bead to be maintained when the solution is introduced to the slot-die head via a feed slot. Various models, including capillary, viscous and viscocapillary, can elucidate the parameters influencing bead and meniscus formation[85]. The characteristics of the coating bead, menisci, film thickness and uniformity depend on the slot-die head configuration. In the slot-die method, the final film thickness is directly proportional to flow rate and solute concentration, but inversely proportional to substrate speed, film width and dry solution density[86]. The temperature of the substrate and air knife influences the film morphology and photovoltaic performance[87]. Although slot-die coating is used to produce perovskite films and components, high-performance PSCs require a more systematic approach and an understanding of fluid dynamics and efficient slot-die designs.

Spray coating is a scalable, low-temperature method for large-area applications, such as multilayered films for tandem applications and flexible PSCs. It involves four successive droplet stages: generation by atomization, transport to the substrate, coalescence into a wet film and drying (Fig. 4h). The size and uniformity of droplets are critical for consistent and uniform films. These variables are influenced by solution properties — such as viscosity and surface tension — alongside nozzle type, flow rate and gas pressure. Maintaining a balance between Bernoulli pressure and surface tension is essential for droplet stability, with droplet size decreasing at lower gas flow rates. Solvent engineering during spray coating can control the crystallization process. Combining a slow-evaporating solvent — for example, γ-butyrolactone — with a fast-evaporating solvent, such as DMF, can help to manage the film morphology and ensure uniform crystallization[88]. Preheating the substrate can improve film quality by controlling the grain size, as higher temperatures produce larger grains[89–91]. Advanced techniques such as megasonic nebulizers can generate smaller and more uniform droplets. Although these approaches have improved performance, it is still challenging to produce highly efficient perovskite films. Compared

Precursor design

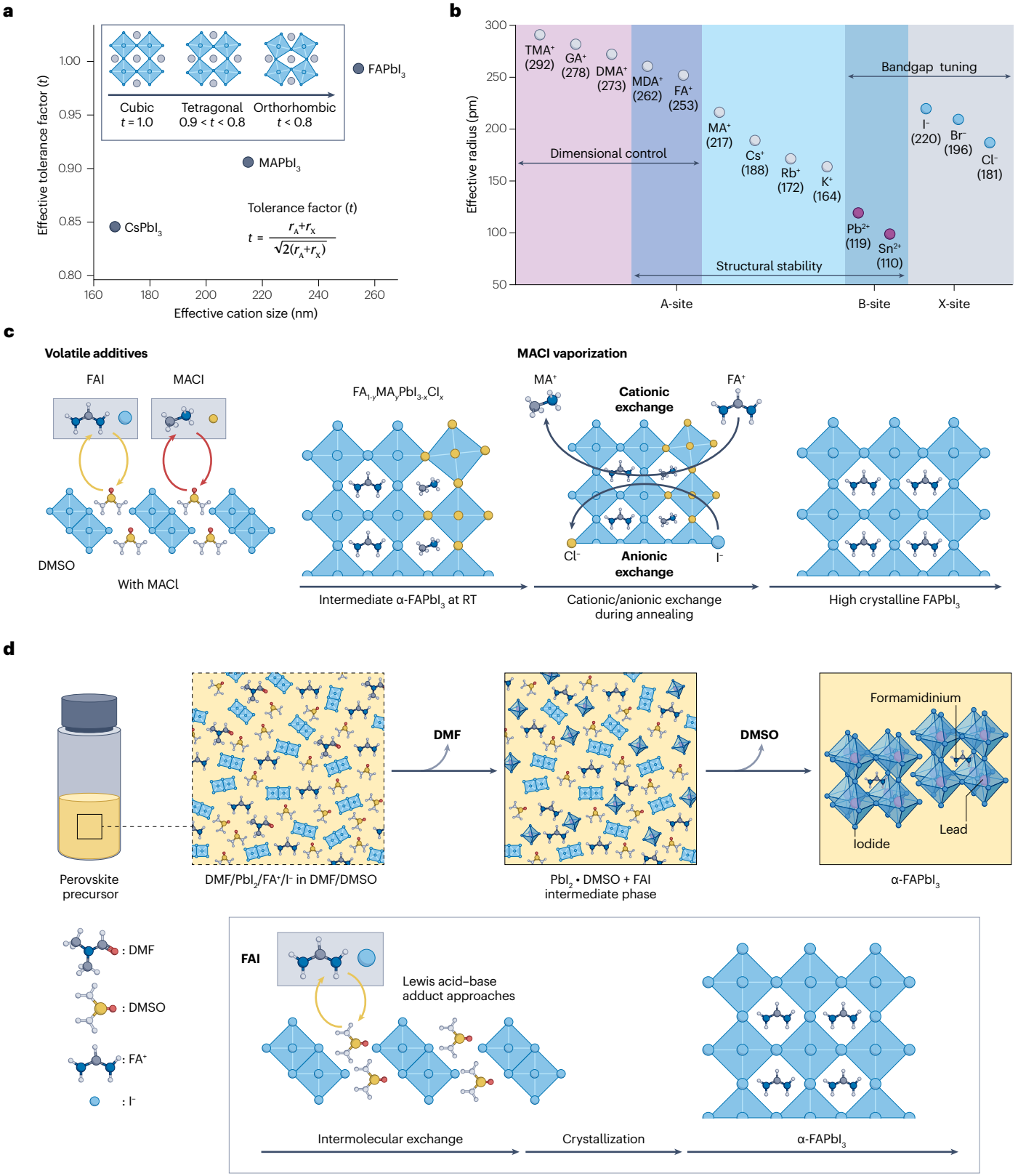

Fig. 3 | Precursor design for common crystallization strategy for α-phase $FAPbI_3$. **a**, Tolerance factor of $CsPbI_3$, methylammonium lead iodide ($MAPbI_3$) and formamidinium lead iodide ($FAPbI_3$), showing that the large size of formamidinium (FA) cation induces a high tolerance factor, close to $t \approx 0.99$. **b**, Effective ionic radii of conventional A-site cations and X-site halides used in compositional engineering to stabilize the α-phase of $FAPbI_3$. **c**, Volatile additive engineering pathway for forming the α-phase intermediate at room temperature (RT) and subsequent cationic/anionic exchange during annealing to achieve highly crystalline $FAPbI_3$. **d**, Solvent engineering strategy by forming Lewis acid–base adducts, facilitating intermolecular exchange and crystallization to form α-$FAPbI_3$. DMF, *N*,*N*-dimethylformamide; DMSO, dimethyl sulfoxide; FAI, formamidinium iodide; MACl, methylammonium chloride.

with slot-die and blade coating, spray coating produces films with lower PCEs and requires further optimization for larger-area coatings.

Inkjet printing offers precise control over droplet placement, making it well suited to applications requiring high customization and minimal material waste. The process involves ejecting small droplets of ink using a pressure pulse produced by a piezoelectric transducer. The precursor ink is propelled towards the nozzle and onto the substrate in a pre-defined pattern[92] (Fig. 4i). Inkjet printing can achieve fine, detailed patterns, down to sub-100 nm scales, making it suitable for PSCs in which precision is essential[93]. A challenge to inkjet printing is the strict ink formulation requirements, including viscosity, surface tension and density[94]. Non-optimized inks can clog nozzles, leading to defects such as missing lines in the printed films. For large-area scalability, inkjet printing is limited by sensitivity to droplet size and ink formulation. Although the technique has produced highly efficient small-area perovskite devices, uniform deposition across larger substrates is harder. This is due to the increased complexity of maintaining consistent droplet size and patterning over larger areas.

By integrating coating techniques — slot-die, blade, spray and inkjet — PSC fabrication can continue to be scaled up. Each technique offers unique advantages and challenges, but the overarching goal is the same: to achieve high-quality, defect-free and highly crystalline perovskite films over large areas suitable for commercialization. A systematic understanding of fluid dynamics, crystallization kinetics and solvent properties is needed to overcome the bottlenecks in scaling up PSC production.

Active layer: lead perovskites from dry methods

An alternative to solution-based techniques is the thermal evaporation method[95]. It has the advantage of being solvent-free, eliminating the environmental and health risks of hazardous solvents using lead-based solutions, such as DMF, DMSO and γ-butyrolactone. It can also fabricate poorly soluble and oxygen-sensitive all-inorganic perovskites, such as $CsPbI_3$ and tin-based perovskites. Dry methods can also achieve conformal coating on textured substrates, which is essential for perovskite–silicon tandem solar cells, and enable fabrication of multilayered perovskite structures not possible by solution processing[96]. Finally, thermal evaporation has better reproducibility and scalability than solution-based methods. Overall, dry processes present a promising alternative to solution-based PSCs as vacuum-based techniques are already established in many industries.

Co-evaporation. In co-evaporation, metal halide and ammonium/inorganic salts are vapourized and deposited onto the substrate simultaneously from separate crucibles to form a perovskite layer (Fig. 5a). Co-evaporation has challenges despite its effectiveness. A major difficulty lies in precisely controlling the deposition rates of organic and inorganic precursors. At a given time, the substrate surface may be occupied by the inorganic precursor, the organic precursor or the perovskite, which hinders uniform deposition. The nucleation and growth mechanisms of dry processes are different to solution processes. Dry processes follow the reaction pathways of Volmer–Weber (adsorbate–adsorbate interactions), Frank–van der Merwe (adsorbate–surface interactions) or Stranski–Krastanov (combined growth mode), which depend on substrate temperature, surface energy and deposition rates[97,98]. Understanding these mechanisms is vital for producing high-quality, stoichiometric perovskite films. Optimizing the evaporation system is also important. For instance, the placement of the quartz crystal microbalance sensor is critical, especially when using omnidirectional flux-emitting organic precursors, such as methylammonium iodide and formamidinium iodide (FAI)[99,100]. To accurately monitor the evaporation rates, the quartz crystal microbalance sensor should be positioned near the substrate[101]. Regular calibration of the deposition rate at a desired chamber condition is crucial for reproducibility. The decomposition of precursors — namely, methylammonium iodide and FAI — during deposition can increase the chamber pressure and cause contamination[102]. The high diffusivity of organic halides can result in deposits on chamber walls that cause stoichiometric imbalances in subsequent batches. To mitigate this, some commercial evaporators use low-temperature cooling systems for the chamber walls and substrates. This can prevent redeposition and control grain size but increases the equipment cost. Co-evaporation also has issues with controlling crystal growth and defect engineering, as the methods used in solution chemistry cannot be directly applied to dry processes[103].

Sequential evaporation. Sequential evaporation, also known as multistep thermal evaporation, is a relatively controllable deposition process that involves stage-wise deposition of precursors (Fig. 5b). Process conditions are optimized for each material, which minimizes complexity in the vapour phase. Substrate temperature, deposition rate and ambient pressure can be tailored for each precursor and the reaction between precursors can be manipulated through post-annealing processes. Higher efficiencies have been reported using sequential processes[104]. Multisource sequential evaporation, where each precursor is deposited sequentially, can simplify deposition rate control. However, this approach requires precise reaction management between precursors to avoid unreacted materials and ensure homogeneous local stoichiometry. Using chloride-based precursors can promote interdiffusion and reaction between precursors[105]. Despite advances, reproducibility and scalability remain a challenge. Further research and optimization are needed to refine process parameters and develop innovative strategies to enhance the consistency and scalability of sequential evaporation processes.

Hybrid deposition. Multistep hybrid deposition combines thermal evaporation with other processes, such as gas-phase and liquid-phase deposition (Fig. 5c). An inorganic salt precursor is thermally evaporated and exposed to an organic halide precursor, triggering a reaction between them. Sometimes, a second step is performed involving chemical vapour deposition (CVD) at low vacuum, where vapourized organic halides are deposited and reacted with inorganic precursors. Alternatively,

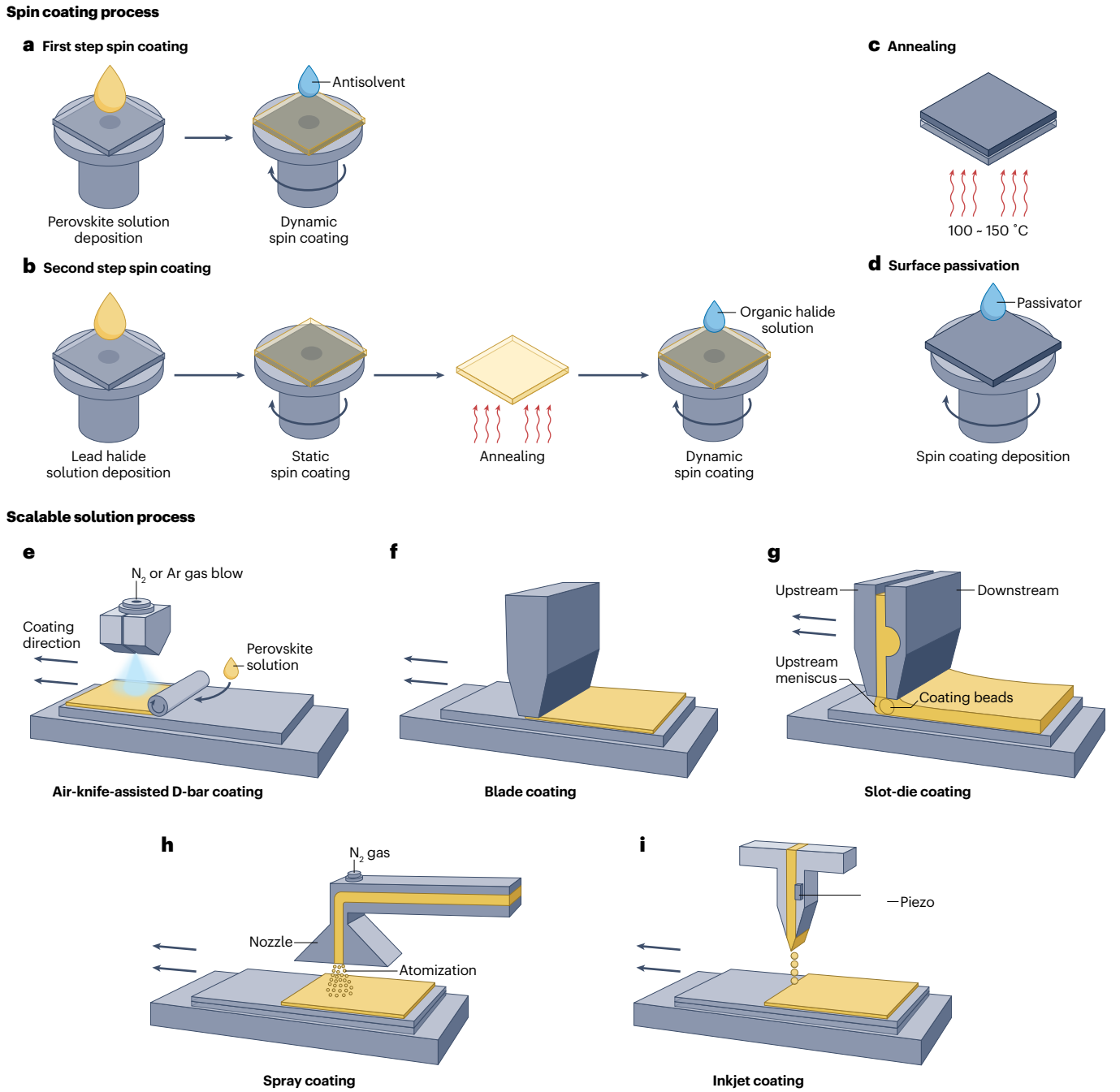

Fig. 4 | Schematic illustration of solution-based perovskite thin film fabrication. a,**b**, Small area perovskite thin film fabrication, with one-step spin coating (part **a**) and two-step spin coating (part **b**). **c**, Annealing process. **d**, Surface passivation process. **e**–**i**, Scalable solution-based perovskite thin film fabrication, with air-knife-assisted D-bar coating (part **e**), blade coating (part **f**), slot-die coating (part **g**), spray coating (part **h**) and inkjet coating (part **i**).

solution methods followed by perovskite thermal evaporation can deposit organic halide precursors. Incorporating solution phase deposition in the hybrid method enables additives to be introduced that are challenging to integrate by thermal evaporation alone. These additives — including hypophosphorous acid, MACl-MABr mixtures or DMSO — can enhance device performance[106–108] and enable record-level PCEs[109].

Active layer: perovskite quantum dots

Perovskite quantum dot (PQD) solar cells offer several advantages over conventional bulk PSCs. Owing to their high surface energy and surface-to-volume ratio, PQDs have enhanced phase stability, inhibiting the transition to photoinactive polymorphs. The bandgap and energy levels of PQDs are readily tuned by varying their sizes. This makes them

versatile for diverse device structures and optoelectronic applications. Fabrication of PQD devices is simpler than bulk PSCs, as it does not require a thermal annealing step. Additionally, the solvents used — nonpolar hexane or octane — are less toxic and more environmentally friendly. Despite these promising attributes, there are several challenges for developing PQD solar cells. The typical capping ligands, oleic acid and oleylamine, are insulating and hinder charge extraction and transport. Incomplete passivation of surface defects leads to carrier trapping and energy loss, an effect exacerbated by the high surface-to-volume ratio of PQDs. Currently, the performance of PQD solar cells, with a record PCE of 18.1%[110], is lower than bulk PSCs.

PQDs can be synthesized by hot injection[111], ligand-assisted reprecipitation[112] and microfluidic synthesis[113]. Hot injection is used most widely to produce high-quality quantum dots with consistent size distribution. In a typical chemical synthesis[111,114], lead-oleate precursors are quickly injected into a heated solution under an inert atmosphere. The solution consists of PbX_2 and ligands dissolved in solvents, such as octadecene. Adjusting the reaction temperature, time and precursor concentration enables size and shape tunability. For device fabrication, PQD thin films are formed using layer-by-layer deposition to achieve the desired thickness (Fig. 6). For photovoltaic applications, ensuring efficient electrical coupling between quantum dots is essential. However, the insulating nature of oleic acid and oleylamine ligands can inhibit charge transport. This is mitigated by using antisolvents in a rinsing process to remove excess ligands and precursors, optimizing the ligand density. Polar antisolvents are chosen to balance solvent polarity and maintain the crystal phase, stability and colloidal integrity of PQDs[65,115,116]. Short-chain esters, such as methyl acetate and ethyl acetate, are preferred[65,114]. Ligand exchange with shorter or conductive species enhances interdot coupling, which may occur during synthesis and deposition stages. Adventitious water is crucial for hydrolysing methyl acetate to facilitate anion ligand exchange by protonating oleate ligands[117–119]. Cation exchange using ammonium halide salts, such as FAI, replaces native ligands, further improving device performance.

Active layer: tin perovskites

The rapid advancement of PSCs has been accompanied by growing concerns over the environmental and health implications of lead ions[120,121]. These toxicity issues challenge the environmental sustainability of PSCs and could limit their industrialization. Strategies to mitigate

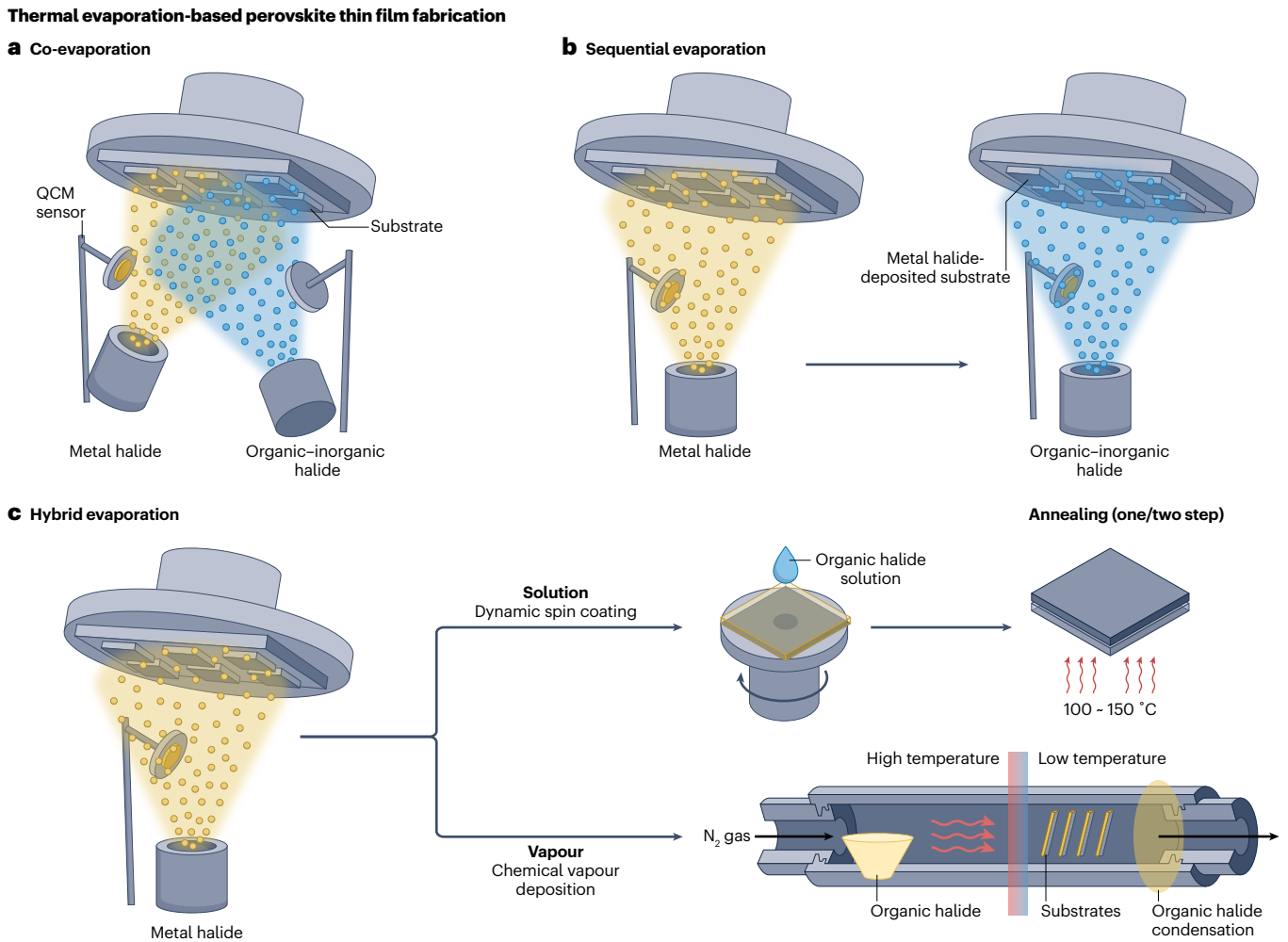

Fig. 5 | Schematic illustration of thermal evaporation fabrication process. Co-evaporation (part **a**), sequential evaporation (part **b**) and hybrid evaporation (part **c**), incorporating solution and chemical vapour deposition. QCM, quartz crystal microbalance.

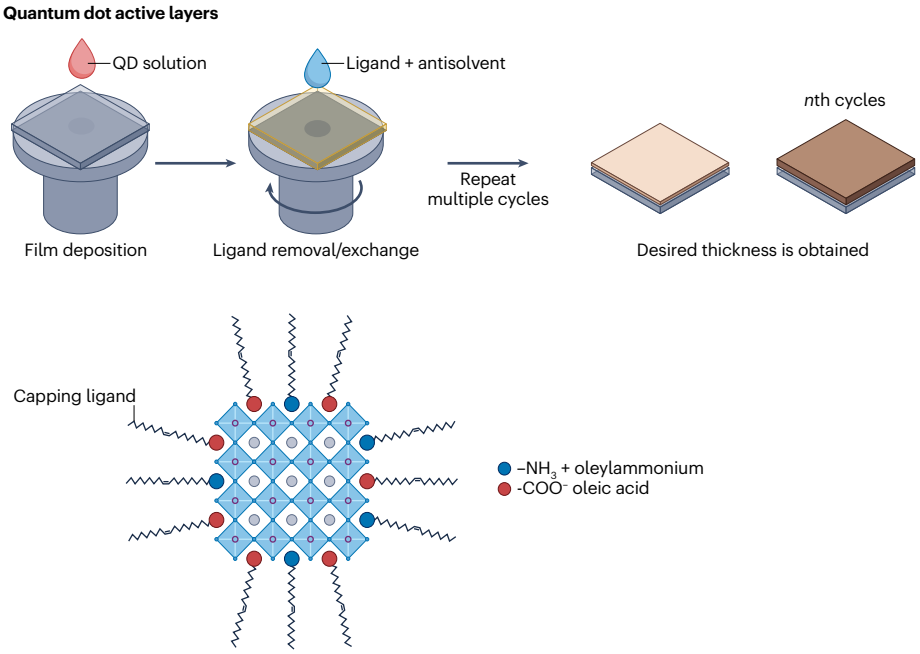

Fig. 6 | Schematic illustration of the fabrication process for a quantum dot active layer. A perovskite quantum dot (QD) thin-film coating process (top). A graphical illustration of the chemical structure of a perovskite QD capped by ligands (bottom).

lead leakage[122–124] have shown promise; however, a comprehensive solution remains elusive. This has driven the search for non-toxic alternatives. Tin-based perovskites are the most promising lead-free candidates over other alternatives such as bismuth and strontium[125–127]. Tin perovskites have lower toxicity, favourable optical bandgaps and high charge carrier mobilities[128,129]. They have smaller bandgaps than lead analogues, giving them the potential to meet theoretical PSC efficiency limits. However, tin-based perovskites are vulnerable to moisture and oxygen. Multiple fabrication methods have been developed to address this challenge, aimed at improving film quality, stability and photovoltaic performance. One-step solution processing uses various A-site cations, such as MA^+, FA^+, Cs^+, AZ^+ (ref. 130), IM^+ (ref. 131) and GA^+ (ref. 132), to enhance the perovskite film quality. Antisolvent dripping, where SnF_2 and $EDAI_2$ (ref. 133) are added during antisolvent dripping, also produces uniform, pinhole-free films. Sequential deposition[134,135] forms a layered structure using bulky ammonium cations and hexafluoro-2-propanol to give a 3D/2D hybrid tin–perovskite film[136]. Most high-performance tin-based PSCs are based on $FASnI_3$ deposited by a one-step method on a hydrophilic HTL poly(3,4-ethylenedioxythiophene):poly(styrenesulfonate), abbreviated to PEDOT:PSS. However, PEDOT:PSS is hygroscopic and can quickly degrade device performance. The reaction between SnI_2 and FAI is fast, making it challenging to replace PEDOT:PSS with other hydrophobic HTLs — such as poly[bis(4-phenyl)(2,4,6-trimethylphenyl)amine] (PTAA) — unless crystal growth can be retarded with a sequential method[137]. Other hole-transport materials (HTMs)[138,139] and self-assembled monolayers (SAMs)[140–142] have successfully replaced PEDOT:PSS in tin-based PSCs. The vapour-assisted method is unique to tin perovskites, in which hydrazine vapour post-treatment[143–145] is used to reduce Sn^{4+} to Sn^{2+}, enhancing overall device stability[127,146,147]. Other methods are analogous to lead-perovskites, for example, the additive strategy in which Lewis bases, such as DMSO, and long-chain organic ammonium compounds assist the oriented slow growth of perovskite crystals by restricting grain tilting[148,149].

Active layer: double perovskites

Double perovskite materials with monovalent and trivalent B-site elements, represented by the general formula $A_2BB'X_6$, are a promising class of compounds for photovoltaics and optoelectronics. These materials such as Cs_2AgBiX_6 offer a potential lead-free alternative to conventional lead halide perovskites[150,151]. The ordered B-site substitution — in which B and B′ are monovalent and trivalent cations, respectively, for instance, Ag^+ and Bi^{3+} — gives better stability against moisture and thermal degradation compared with lead-based counterparts[152]. Double perovskites typically have wider and indirect bandgaps, such as 1.95 eV in $Cs_2AgBiBr_6$. This potentially limits single-junction solar cell efficiency but is advantageous for perovskite–perovskite tandem cells and radiation detection[153,154]. Lead–tin double perovskites are promising for mitigating the toxicity of lead-based perovskites while maintaining high performance. These materials, typically formulated as $FA_{1-x}Cs_xPb_{1-y}Sn_yI_3$, enable partial substitution of Pb^{2+} with Sn^{2+}, reducing the lead content by up to 50% without significantly compromising device efficiency[155]. Lead–tin double perovskites have extremely narrow bandgaps — down to ~1.2 eV — compared with other double perovskites, enhancing light absorption in the near-infrared region[156]. This characteristic makes them particularly attractive for tandem solar cell applications, in which they can be paired with wide-bandgap perovskites or silicon[157]. However, double perovskites have lower absorption coefficients and less efficient charge transport than regular perovskites. These limitations may be overcome with compositional engineering, by varying B and B′ cations and halide alloying. In particular, heterovalent substitution can optimize electronic properties, enhance charge mobility and improve solar cell PCE. This could lead to new applications beyond photovoltaics, including light-emitting diodes and other optoelectronic devices[158,159].

Charge-selective layer: metal oxides

Solution methods. Metal oxide-based thin films are typical charge transport layers in optoelectronics. This is due to their optical transparency,

mechanical robustness and solution processability. PSCs also use metal oxide ETLs, such as TiO_2 and SnO_2, which are favoured for n–i–p-structured PSCs. These oxides can be synthesized using solution-type methods, namely, spin-coating and slot-die coating, followed by thermal annealing[160] (Table 2). It requires extremely high-temperature annealing (~500 °C), which limits flexible substrate applications. In addition, TiO_2 has high chemical capacitance and UV-induced photocatalytic degradation. Strategies to enhance the performance of TiO_2 include morphological optimization, doping and surface treatments[161–164]. By contrast, SnO_2 has a lower annealing temperature of ~150 °C, making it suitable for flexible PSCs, with a larger bandgap (3.6–4.0 eV) and higher electrical conductivity than TiO_2 (ref. 165). SnO_2 is typically deposited via colloidal nanoparticles[166], chemical bath deposition (CBD)[31,167] or spray pyrolysis[168]. CBD can produce denser films with fewer defects than conventional spin-coating methods but requires longer post-treatment times. Another metal oxide ETL, ZnO, was initially used widely in organic solar cells. However, it is highly reactive with perovskites, diminishing the initial hype[169]. For HTL p-type metal oxides, nickel oxide (NiO_x) is prominently used, as it has a wide bandgap and high open-circuit voltage (V_{oc}), giving high PCE when used in devices[170–172]. The synthesis and fabrication of NiO_x influence the device performance. Solution-type methods, such as spin coating[170,173,174], spray pyrolysis[175], CBD[176] and electrochemical deposition[177], can be used to deposit NiO_x, whereas dry-type methods, such as ALD[178], magnetron sputtering[179], pulsed laser deposition[180] and electron beam evaporation[181] are also viable options.

Dry methods. Dry-type methods can fabricate metal oxide charge-selective layers, including NiO_x, TiO_x, SnO and ZnO. These approaches typically have higher costs, longer processing times and size limitations; however, they generally produce better-performing PSCs than solution-type methods. This is because dry methods result in greater crystallinity and fewer impurities. Solution deposition may also damage substrates and underlying layers owing to solvent interactions. They also have limited uniformity on rough or textured surfaces, which is crucial for tandem applications. Additionally, in solution, control over the thickness of a metal oxide film is constrained to several tens of nanometres[182,183]. Dry-type methods, such as ALD and sputtering, circumvent these issues. They produce amorphous and more compact metal oxide films of higher quality at RT, enabling flexible applications[184–187]. For instance, a PCE of 23.4% was achieved in inverted PSCs using electron-beam-evaporated NiO_x combined with surface redox engineering using argon plasma and acid treatment[188,189]. Further doping and meticulous interface engineering optimized the NiO_x (refs. 190–194). SnO_2 thin films, characterized by wide bandgap and high carrier mobility, can also be produced using dry-type methods, such as ALD[195,196]. These techniques offer precise control over film thickness and produce high-quality, pinhole-free layers at low temperatures[197–199]. The highest efficiency of perovskite tandem solar cells currently use an ALD SnO_2 buffer overlayer within the p–i–n architecture[200]. Typically, H_2O[201], O_2 plasma[202] and O_3 (ref. 196) serve as oxygen sources to form Sn–O bonds using tetrakisdimethylamino tin as a tin precursor. Innovative low-temperature ALD processes use H_2O_2 as an oxygen source to reduce surface defects and improve the SnO_2/perovskite interface, enhancing overall device performance and stability[203,204]. Sputtering ZnO under high working pressures improves crystallinity and reduces surface imperfections. This is because the high working pressure moderates the energy of incoming high-energy particles, such as argon, by controlling the bombardment energy. As a result, ZnO-based PSCs have higher PCEs and enhanced device longevity[169].

Charge-selective layer: organic materials

Solution methods. Organic materials are attractive candidates for charge-transporting layers in optoelectronics as they are chemically tuneable, mechanically flexible and easily processed in solution[205]. Unlike metal oxides, organic materials do not require post-treatment, streamlining the production process. Spiro-MeOTAD is used widely in n–i–p PSCs owing to its favourable band alignment and straightforward processing[206–208]. However, there are challenges when using spiro-MeOTAD. For example, chemical doping agents, such as lithium bis(trifluoromethanesulfonyl)imide (Li-TFSI) and tert-butylpyridine

Table 2 | Charge-selective layer materials and fabrication methods for perovskite solar cells

	Materials	Role	Solution methods	Dry methods
Metal oxide	TiO_2	ETL	Spin coating, doctor blade	ALD, CVD, sputtering
	SnO_2	ETL	Spin coating, CBD	ALD
	ZnO	ETL	Spin coating	Sputtering
	NiO_x	HTL	Spin coating, spray pyrolysis	ALD, sputtering
Organic materials	Spiro-MeOTAD	HTL	Spin coating	–
	Polymeric HTL (PEDOT:PSS, P3HT, PTAA)	HTL	Spin coating, inkjet printing, slot-die coating	–
	Fullerenes	ETL	Spin coating	Thermal evaporation
	PCBM	ETL	Spin coating	–
	SAMs	Surface passivation and hole selective interface layer	Dip coating, spin coating	–
	BHT	Additive for stability and hole transport improvement	Spin coating (as an additive to HTL)	–

ALD, atomic layer deposition; BHT, dibutylhydroxytoluene; CBD, chemical bath deposition; CVD, chemical vapour deposition; ETL, electron transport layer; HTL, hole transport layer; NiO_x, nickel oxide; P3HT, poly(3-hexylthiophene-2,5-diyl); PCBM, [6,6]-phenyl-C_{61}-butyric acid methyl ester; PEDOT:PSS, poly(3,4-ethylenedioxythiophene); PTAA, poly[bis(4-phenyl)(2,4,6-trimethylphenyl) amine]; SAM, self-assembled molecule; SnO_2, tin dioxide; spiro-MeOTAD: 2,2′,7,7′-tetrakis[*N*,*N*-di(4-methoxyphenyl)amino]-9,9′-spirobifluorene; TiO_2, titanium dioxide; ZnO, zinc oxide.

(*t*-BP), are needed to enhance hole mobility. These dopants are typically applied through spin coating or drop casting on perovskite films[209,210]. Although these additives are crucial for improving charge transport, they introduce critical components that contribute to degradation and lower thermal stability[211–215].

In p–i–n PSCs, PEDOT:PSS is used as an HTL owing to its high electrical conductivity and transparency[216,217]. However, it can only be used for inverted-type PSCs as it is an aqueous solution, which dissolves perovskite layers. PEDOT:PSS is typically applied by spin coating or inkjet printing to form ultra-thin layers[218,219]. However, PEDOT:PSS is hygroscopic and can degrade perovskite films when exposed to ambient conditions, reducing device stability. Alternative polymeric HTLs, such as poly(3-hexylthiophene) (P3HT) and PTAA, offer improved stability against thermal stress and moisture compared with PEDOT:PSS. These polymers are also restricted to solution-type deposition processes. However, their solubility in nonpolar solvents means that they can be deposited on the perovskite layer, although their energy levels mean that they can be used in both standard and inverted PSC configurations. P3HT has lower transparency than PTAA and is more frequently used in p–i–n structures, despite its sensitivity to UV light. There is a need to balance optical properties, charge transport capabilities and long-term stability when selecting HTL materials. New HTL materials or innovative deposition techniques may be needed to overcome the trade-offs between efficiency, stability and processability. In inverted PSCs, the electron transfer layer — [6,6]-phenyl-C_{61}-butyric acid methyl ester (PCBM) — is a challenge to enhance owing to surface defects and charge recombination. To address these issues, various buffer layers have been explored, including bathocuproin (BCP)[220,221], zirconium acetylacetonate ($Zr(ac)_4$)[222], calcium acetylacetonate ($Ca(acac)_2$)[223] and lithium fluoride (LiF)[224]. After the BCP overcoating concept was introduced to the perovskite community, BCP was applied to inverted-type PSCs via spin coating, with BCP dispersed in ethanol. This method risks damaging the underlying layer, despite using high-speed spin-coating techniques. Now, BCP is predominantly deposited using thermal evaporation, which minimizes damage and gives controlled, uniform layering.

Fullerenes, including C_{60} and C_{70}, are nanocarbon materials that occupy a unique position between organic and inorganic materials. They are effective ETLs that enhance V_{oc} and reduce photocurrent hysteresis compared with metal oxide ETLs[225–228]. These materials can be processed using both solution-type and dry-type methods[229–232]. In the solution approach, the limited solubility of fullerenes means that vacuum drying is needed to improve film quality after solution coating, remove remnant solvents and consolidate packing[233,234]. Functionalization of fullerenes by attaching addends improves their solubility and ability to permeate the underlying film, thoroughly passivating defects[233–240]. Fullerene species are used as standalone ETLs, as supplementary overcoats to metal oxide ETLs[8,240] or as dopants for charge transporting layers[240–242].

SAMs are applied by vapour or liquid-phase deposition, forming thin molecular layers on a substrate[243,244]. SAMs reduce interfacial traps and enhance charge carrier transfer, making them ideal as hole-selective contacts in inverted PSCs. SAMs typically have three main components: an anchoring group to establish a chemical bond with the substrate; a connective linker that determines the packing geometry; and a terminal functional group to customize surface and interfacial properties[200,245–247]. SAMs have minimal parasitic absorption, are scalable and cost-efficient, making them effective for large-area PSCs.

Dibutylhydroxytoluene (BHT), a common antioxidant and stabilizer for commercial polymers[248,249], can be used to stabilize or modulate growth in PSCs. BHT is incorporated during film formation by mixing it into the precursor solution. It aggregates at grain boundaries, reducing ion migration[250–252]. The counter anion in BHT molecules may also interact with the perovskite precursor, modulating growth kinetics[253,254].

Dry methods. Fullerene, C_{60}, has denser packing, higher electron mobility and greater conductivity than PCBM. However, forming high-quality thin films of C_{60} is challenging owing to low solubility and hydrophobicity[255,256]. To address this, high-quality crystalline C_{60} thin films are fabricated through vacuum thermal evaporation, with slow evaporation rates and degassing of the C_{60} powder under high vacuum. This ensures minimal kinetic energy loss and enhanced film quality[257–259]. Before deposition, the C_{60} (99%) powder should be degassed at 200 °C under high vacuum for several hours to eradicate absorbed impurities and residual solvent. Consequently, preparing high-quality C_{60} thin films by sublimation is a time-intensive process. The process of thermal evaporation requires a hot source material to be generated and deposited as a thin film on the substrate. Using an ultra-high vacuum environment during thermal evaporation can diminish the kinetic energy lost by evaporated particles, enhancing the resulting thin film quality[160,260–263].

Electrode layers

Transparent bottom electrodes. Electrodes are crucial components in PSCs. To achieve optimal performance, at least one electrode must be transparent to allow light interaction with the photoactive perovskite layer. Metal oxide-based transparent conductors, namely, indium tin oxide and fluorine-doped tin oxide, are commonly used in PSCs. These electrodes are often fabricated using radiofrequency sputtering followed by high-temperature post-treatment to ensure compactness and maximize DC-to-optical conductivity. Although this method is suitable for glass substrates, fabricating flexible devices and tandem solar cells for building-integrated photovoltaics (BIPV) applications is challenging. The deposition process can potentially damage underlying layers and high-temperature post-treatment restricts device performance optimization. Metal oxide films have limited flexibility, with cracks appearing at bend angles of ~60° (refs. 264,265). The current trend towards foldable and stretchable electronic products[266,267] makes this an important challenge to address.

An alternative for transparent electrodes is to use a metal mesh. These meshes offer high conductivity, whereas aerial voids ensure high transparency[268,269]. However, the costly patterning process of sputtering and etching, coupled with metal ion migration-driven perovskite degradation, has limited widespread adoption. A solution-based variant is metallic nanowires (MeNWs), which have widths of a few tens of nanometres and lengths on the micrometre scale. Successful demonstrations have been achieved using silver[270,271], copper[272,273], gold[274] and nickel[275]. Despite their low cost and excellent DC-to-optical value, the rough film surface and metal ion migration-driven degradation mean this approach is now less explored.

Carbon electrodes, namely, graphene and carbon nanotubes (CNTs), are alternatives that offer better mechanical flexibility than conventional electrodes, enabling foldable and crumplable PSCs[276–278]. Neutral colouring and the low haze of carbon electrodes offer further advantages. Graphene and CNTs can be transferred onto substrates by dry or solution approach[279,280]. Thermal tape can be used for dry electrode transfer of graphene from copper; however, remnant adhesives need to be removed in an H_2-containing oven[281]. A more common choice is to dip the substrate in an acid bath to dissolve copper foil while the

graphene is afloat. Systemizing this method in a pilot line enables large sizes and a roll-to-roll process[282]. CNT transparent electrodes are promising in PSCs[283,284]. Single-walled CNTs produced by floating-catalyst CVD (FCCVD) for the dry transfer and double-walled CNTs for the solution process have demonstrated the best performance in PSCs[285,286]. Despite slightly rougher morphology and lower transmittance than graphene, FCCVD-based CNTs have superior reproducibility, stretchability and a facile transfer process[287,288].

Top electrodes. Metal electrodes in PSCs are typically deposited using thermal evaporation in vacuum; a dry method prevalent in small-scale laboratory settings. This technique involves heating metal in a vacuum until it sublimates. The resulting metal vapour condenses on a cooler perovskite or charge-selective layer to form a thin, uniform metallic film. Commonly used metals include gold, silver, aluminium and copper. Thermal evaporation offers excellent control over film thickness and purity but requires high vacuum conditions and is relatively energy-intensive. In industrial settings, sputtering is preferred as it can produce highly uniform thin films over large areas, despite being more complex and costly than thermal evaporation. A more economical and straightforward solution-based approach is to use silver paste or eutectic gallium–indium alloy, but this is disfavoured as it can damage the sensitive perovskite layer and limit electrical conductivity[289,290]. Other more peripheral methods include electrodeposition, also known as electroplating, in which an electrochemical process deposits metal from a metal salt solution onto the perovskite surface[291,292].

Metal electrodes are gradually being phased out from PSCs. Their fabrication, which requires vacuum conditions for thermal evaporation, consumes a large amount of energy, hindering scalability and commercial viability. Carbon-based counter electrodes (top electrodes), such as CNTs and carbon paste, are emerging as novel, cost-effective alternatives[293–296]. There are unique challenges when preparing top electrodes. Any physical, thermal or chemical damage to the underlying layers, especially the sensitive perovskite layer, must be avoided during electrode deposition. There are two primary alternatives: free-standing FCCVD CNTs and carbon pastes. FCCVD CNT films can be directly laminated onto the perovskite layer without solvents or thermal annealing and are semi-transparent, enabling tandem applications[294,297]. Carbon paste is another promising nanocarbon electrode. For carbon paste-based PSCs, the perovskite solution is typically formed after deposition of the carbon paste electrode. These devices have a higher PCE, but with greater stability compared with that of FCCVD CNT-based devices. However, carbon paste electrodes are more than 10 times thicker than CNT electrodes, require high-temperature processing (~500 °C) and are completely non-transparent. This limitation means that they cannot be used for tandem, BIPV or flexible applications. Both types of nanocarbon top electrodes are abundantly available, exhibit high electrochemical stability and have superior hole extraction capabilities. The p-type electrical conductivity of carbon materials, combined with their exceptional chemical inertness, makes them particularly well suited to this application[298–300]. Overall, carbon-based electrodes could lower manufacturing costs, improve device stability and reduce carbon dioxide emissions by using carbon dioxide as a starting material[296,301].

Results

Assembly into device

PSCs, whether normal or inverted architecture, have a consistent layered assembly structure. This structure comprises a substrate, transparent electrode, charge-selective layer, perovskite layer, another charge-selective layer and a top electrode. An exception occurs when using a carbon-based top electrode, which may be laminated before the perovskite or charge-selective layer. The assembly process begins by selecting a substrate. Although glass substrates are traditionally used, polymer substrates are essential for flexible PSCs. Following substrate selection, the remaining layers are sequentially deposited using either dry or solution methods. Dry deposition methods can cause damage to underlying layers through high temperatures, physical bombardment or lamination pressure. By contrast, solution methods require careful consideration of solvent compatibility. Nonpolar solvents are typically preferred for depositing layers above the perovskite, as polar solvents can dissolve the perovskite layer. Throughout the assembly process, maintaining layer integrity is crucial. Each new layer must be deposited without compromising the structure or function of underlying layers. This requirement constrains the choice of materials and fabrication methods. The selection of materials must account for their compatibility with adjacent layers and the deposition processes used. The complex interplay between material properties and fabrication techniques underscores the importance of careful process design in PSC fabrication. Balancing these factors is essential for achieving high-performance solar cells.

Perovskite active layer analysis

Morphological and compositional characterization. To probe the morphology and composition of perovskite films at various scales, a suite of advanced characterization techniques is available. At the nanoscale, atomic force microscopy (AFM) can provide high-resolution, 3D images of surface topography, revealing details such as grain size, surface roughness and the presence of defects. Extending this capability further, conductive AFM enables simultaneous measurement of local electrical properties to probe conductivity variations and defect-related electronic behaviour at the nanoscale. Scanning electron microscopy can visualize the surface and cross-sectional morphology of perovskite films. From this, grain boundaries, film uniformity and layer thickness can be investigated. These factors are essential to correlate structural features with device performance. For atomic-level imaging, transmission electron microscopy can reveal crystallographic information and identify defects, dislocations, and phase purity. However, beam-induced damage should be avoided by optimizing sample preparation and measurement conditions[302]. X-ray diffraction is widely used to determine the crystallographic structure and phase composition of perovskite films. This method excels at identifying different crystalline phases, quantifying crystallinity and detecting secondary phases. Complementing these structural characterization techniques are spectroscopic methods that can derive the optical and chemical properties of a perovskite film. Ultraviolet–visible (UV–Vis) absorption spectroscopy, for instance, elucidates the optical absorption properties, whereas Fourier-transform infrared spectroscopy identifies vibrational modes in the perovskite structure. These techniques provide valuable information about chemical compositions and atomic interactions within the films.

Optical characterization. Photoluminescence spectroscopy is fundamental for studying charge carrier recombination processes in perovskite films. It offers insights into the bandgap, defect states and overall material quality. Time-resolved photoluminescence extends this capability by measuring the decay dynamics of photoluminescence, providing information on charge carrier lifetimes and the efficiency of radiative recombination. UV–Vis spectroscopy is a useful

and accessible method to determine bandgaps and degradation rates. Photothermal deflection spectroscopy offers further insights by quantifying the energetic disorder, known as the Urbach energy, and density of sub-bandgap states.

Electrical characterization

The performance of electrodes in PSCs depends on a delicate balance between electrical conductivity and optical transparency. An ideal electrode will have high electrical conductivity for efficient charge transport and superior optical transparency to maximize light transmission to the active layer. To quantitatively assess electrical conductivity, four-point probe measurements are used. This technique provides a precise determination of sheet resistance, offering valuable insights into the conductive properties of electrode. The transparency of electrodes is typically evaluated using UV–Vis spectroscopy. This assessment shows that it is needed to determine light-harvesting capabilities, particularly within the visible spectrum. Although these measurements offer notable insights, they are not exhaustive. The space-charge-limited current method is used to characterize the trap density and mobility of perovskite films. However, artefacts caused by ion migration and the electrode fabrication process can skew results[303].

Power output measurement

Current–voltage (*I*–*V*) measurements are crucial for determining PCE and identifying the maximum power point of PSCs (Fig. 7). Unlike silicon solar cells, which generally exhibit stable *I*–*V* characteristics, PSCs are susceptible to hysteresis and transient behaviours[304,305], giving simpler PCE measurements[306]. Stabilized power output measurements under constant bias and illumination are essential for PSCs. External quantum efficiency and incident photon-to-electron conversion efficiency measurements are also vital, providing a spectral response by measuring the fraction of incident photons converted to electrons at each wavelength. Integrating the external quantum efficiency over the solar spectrum gives J_{sc}, which should be matched with the *I*–*V* measurement using a spectral mismatch correction.

Mechanical characterization

Mechanical testing is essential to evaluate the durability and robustness of PSCs, particularly for flexible and wearable applications. Nanoindentation gives the mechanical resistance to deformation and ability to withstand mechanical stresses. For flexible PSCs, cyclic folding tests assess mechanical endurance. This method involves repeatedly folding the solar cell substrate to evaluate performance after multiple bending cycles. Universal testing machines are used for tensile and compression testing of PSCs. These machines apply controlled forces to samples and measure their response, providing data on tensile strength, elongation at break and Young's modulus. Comprehensive mechanical characterization is crucial for developing PSCs that can withstand real-world applications.

Interfacial characterization

Interfaces are important in determining the overall device efficiency, stability and charge transfer dynamics[307–309]. The multilayered structure of PSCs, in which the perovskite absorber is sandwiched between transport layers, means the interfacial contact quality between layers is critical for optimizing charge extraction and reducing losses. Interactions at interfaces directly impact the optoelectronic properties of the device, such as the V_{oc} and fill factor, which are sensitive to the energy band alignment and interfacial defects. Characterizing interfaces is crucial to understand the underlying mechanisms behind charge transfer, recombination and stability. It provides insights into the chemical, structural and electronic properties, helping to identify defects and study how energy levels align between the perovskite and adjacent layers. From this information, targeted improvements can be made in interface design to enhance device performance. Many characterization techniques are used to analyse different aspects of PSC interfaces. Table 3 summarizes these techniques, detailing their capabilities for analysing carrier dynamics, surface morphology, chemical composition and charge transport behaviour. For instance, time-resolved photoluminescence and electrochemical impedance spectroscopy are used to study carrier lifetimes and charge transport dynamics. These techniques explore the temporal aspects of charge behaviour, which is needed to understand the efficiency of charge separation and transport across interfaces. Surface morphology, a critical factor in interfacial contact quality, is often probed using AFM. Using AFM, nanoscale resolution of surface features can be obtained, showing how the physical structure at an interface affects charge transfer and recombination. Chemical composition and electronic states at interfaces are typically investigated using X-ray photoelectron spectroscopy. For more detailed analysis, high-resolution transmission electron microscopy

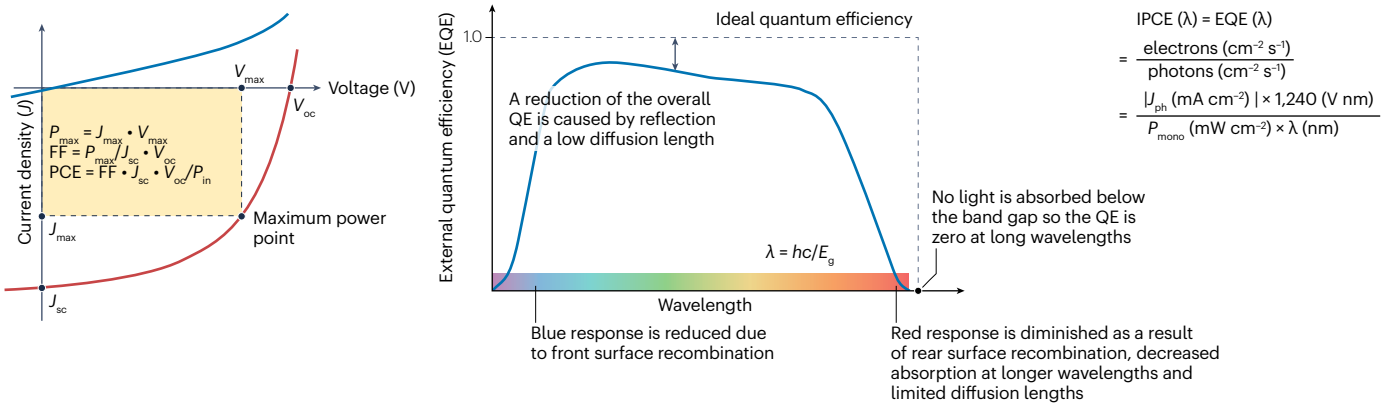

Fig. 7 | A typical current density–voltage (*J*–*V*) curve and quantum efficiency spectrum as a function of wavelength. Incident photon-to-electron conversion efficiency (IPCE) and external quantum efficiency (EQE) were calculated using the formula on the right. λ, wavelength; FF, fill factor; J_{ph}, measured photocurrent value; PCE, power conversion efficiency; P_{max}, electrical peak power; P_{mono}, power intensity of light irradiated at a single wavelength; V_{oc}, open circuit voltage.

Table 3 | Characterization techniques for perovskite solar cells and their advantages and disadvantages

Technique	Measurement	Functions and recent advances	Advantages	Disadvantages
Time-resolved photoluminescence (TRPL)	Carrier dynamics, recombination rates	Improved time resolution for capturing fast carrier lifetimes	Provides detailed insights into charge carriers	Limited spatial resolution, cannot directly map spatial variation
Electrochemical impedance spectroscopy (EIS)	Charge transport, interface resistance	Enhanced sensitivity for probing low-frequency phenomena	Excellent for studying interface properties and charge transport at different frequencies	Requires complex data interpretation and fitting
Atomic force microscopy (AFM)	Surface morphology, topography	High-resolution AFM modes like peak force tapping and conductive AFM for detailed electrical mapping	High spatial resolution for surface analysis can map topography at the nanoscale	Requires ultra-thin sample preparation, potential for electron beam damage
High-resolution transmission electron microscopy (HRTEM)	Interface structure, grain boundaries	Atomic-scale imaging of interfaces with sub-ångström resolution	Provides direct visualization of atomic arrangements at interfaces, especially grain boundaries	Requires ultra-thin sample preparation, potential electron beam damage
X-ray photoelectron spectroscopy (XPS)	Chemical composition, oxidation states	Depth profiling combined with angle-resolved XPS to study surface and interface chemistry. Can detect halide migration and interface degradation	Highly sensitive to surface chemical composition and oxidation states, useful for detecting degradation, elemental distribution and chemical bonding	Surface-sensitive, limited depth (up to ~10 nm) and requires complementary techniques for deeper layer analysis. Sample damage possible during sputtering
Kelvin probe force microscopy (KPFM)	Surface potential, work function	Improved resolution for potential mapping at the nanoscale	Capable of mapping surface potential and charge distribution with high spatial resolution	Sensitive to environmental conditions, such as humidity
Scanning electron microscopy (SEM)	Surface morphology, cross-sectional views	Enhanced detectors for better resolution of nanostructured interfaces	Ideal for surface and interface imaging, particularly useful for cross-sectional views of thin films	Limited chemical information, cannot probe below surface features
Time-of-flight secondary ion mass spectrometry (ToF-SIMS)	Elemental distribution, depth profiling	Improved lateral and depth resolution to detect trace elements and complex compounds	High sensitivity to surface and near-surface regions, excellent for detecting trace elements, isotopic ratios and degradation pathways	Limited to surface layers unless using depth profiling, costly instrumentation and quantitative analysis is challenging due to matrix effects
Grazing incidence X-ray diffraction (GIXRD)	Crystal orientation, strain at interfaces	In situ GIXRD to monitor changes during device operation or thermal cycling	Non-destructive, provides detailed information on thin film structure and interface quality	Complex data interpretation, often requires synchrotron facilities
Electron beam-induced current (EBIC)	Charge collection efficiency, recombination sites, buried interface mapping	Improved spatial resolution, integration with SEM for detailed mapping of local charge collection efficiency and defects across interfaces	Provides direct visualization of charge collection and recombination sites, particularly at buried interfaces and can identify defects affecting local device performance	Requires a vacuum, complex sample preparation and sensitive to beam-induced damage
Transient photovoltage (TPV)	Charge carrier lifetime, recombination dynamics	Improved time resolution, enabling analysis of carrier lifetimes with greater precision under varied illumination and bias conditions	Insights into recombination processes and charge carrier lifetimes	Sensitive to experimental conditions, requires careful control and complex data interpretation
Transient photocurrent (TPC)	Charge extraction dynamics, carrier mobility, response time	Enhanced analysis of charge extraction efficiency and speed, particularly useful for studying interfacial charge transfer processes in perovskite solar cells	Directly measures the dynamics of charge carrier extraction to evaluate the quality of interfaces and transport layers	Requires precise control of illumination and device bias conditions. Complex data interpretation requiring kinetic models

can reveal the atomic-scale crystalline structure at interfaces and any defects that could impact device performance. Time-of-flight secondary ion mass spectrometry has unparalleled capabilities for mapping elemental distributions across interfaces, revealing how elements migrate or segregate. This is valuable information to understand degradation mechanisms and stability issues in PSCs.

Applications

The versatility of PSCs makes them key in future renewable energy technologies, with applications ranging from urban infrastructure to advanced space missions. A primary application of PSCs is in BIPV, in which they can be incorporated into windows, façades and rooftops, transforming buildings into energy-generating structures. The semi-transparent nature of some perovskite materials makes them particularly suitable for this application, enabling light transmission while generating electricity[310]. Another promising application is in portable and flexible electronics. Owing to their lightweight and flexible nature, PSCs can be integrated into wearable devices, mobile chargers and other portable power sources, providing a reliable and sustainable energy supply[311]. PSCs are being explored for use in tandem solar cells,

which are stacked on traditional silicon solar cells to achieve higher overall efficiencies. This tandem configuration can surpass the efficiency limits of single-junction cells, making it promising to maximize energy harvesting[312]. Additionally, PSCs are used in space technologies owing to their high power-to-weight ratio, radiation hardness, high PCEs under a wide range of light intensities and robustness under intense radiation. As a result, PSCs are an attractive option to power satellites and other space-based applications[313,314].

Perovskite–silicon tandem solar cells

Perovskite–silicon tandem solar cells, particularly in two-terminal configurations, could be rapidly commercialized if they surpass the efficiency limits of traditional single-junction silicon cells. Tandem cells capitalize on the complementary properties of perovskite and silicon, combining the superior visible light absorption of metal halide perovskites with the efficient infrared absorption of silicon. This synergy enables PCEs over 30%, substantially higher than the 26% theoretical maximum of single-junction silicon cells. Consequently, this technology reduces the levelized cost of electricity and enhances the competitiveness of solar energy[315–317]. A key advantage for commercialization is that perovskite–silicon tandem cell fabrication is compatible with existing silicon manufacturing processes. The mature silicon cell production industry has an established infrastructure that could integrate perovskite layers through low-temperature, solution-based deposition methods. This alignment facilitates a smoother transition from laboratory-scale production to industrial-scale manufacturing, minimizing the need for new production facilities and accelerating market entry. Recent advances in perovskite material stability and durability address previous concerns about long-term performance. Improved compositions and encapsulation techniques have enhanced resistance to environmental degradation[318], which is crucial to achieve the operational lifetimes required for commercial viability, potentially matching or exceeding those of traditional silicon cells.

The momentum behind perovskite–silicon tandem technology is enhanced by investment from both academia and the photovoltaic industry. Several companies have initiated pilot production lines — for example, PEPPERONI, TEAMUP and ADDEPT — demonstrating the potential for large-scale deployment by increasing efficiency certifications and scaling production capabilities. The market potential of perovskite and silicon technologies is synergistic rather than competitive. Although silicon cells are well established for their durability and reliability, perovskites provide higher efficiency and cost-effective versatility. Integrating these technologies in tandem cells takes advantage of their respective strengths. As a result, there is a strategic future path with perovskite–silicon tandem cells dominating high-efficiency markets and silicon cells serving cost-sensitive applications. The gradual integration of perovskite technology suggests a promising future for solar energy, combining the best of both worlds to drive innovation and sustainability.

Device stability: a commercialization bottleneck

The commercial viability of PSCs and tandem solar cells depends on a thorough assessment of their long-term stability under real-world conditions. Stability is a challenge for PSCs, as they are sensitive to environmental stressors, such as heat, light, moisture and mechanical stress. Degradation mechanisms, including ion migration and phase segregation, are particularly problematic. Ion migration occurs under continuous light exposure and involves the movement of halide ions in the perovskite layer towards interfaces. This phenomenon leads to a decline in performance and defect formation[67,319–321]. In mixed-halide perovskites, phase segregation results in the separation of bromide and iodide to form regions that lower the effective bandgap and reduce overall efficiency[322–324]. The mismatch in thermal expansion between perovskite and silicon layers can induce mechanical strain, leading to cracking or delamination, further compromising device integrity[325,326]. To ensure commercial readiness, rigorous stability assessments for PSCs and tandem solar cells must be conducted using standardized protocols, such as those defined in IEC61215, which is international standard for testing and certifying solar photovoltaic modules published by the International Electrotechnical Commission (IEC)[327–330]. These protocols address critical environmental stressors, including heat, light and moisture. However, modifications are necessary to account for the specific degradation mechanisms of perovskite-based devices, such as ion migration and phase segregation. The 2018 International Summit on Organic PV Stability (ISOS) introduced tailored protocols for PSCs, emphasizing light soaking and thermal cycling tests[331,332]. These tests replicate extended sunlight exposure and temperature variations to evaluate the retention of PCE. Encapsulation has shown promise in enhancing stability — with encapsulated PSCs retaining more than 95% of their initial efficiency after 1,000 h of light soaking[200] — but still falls short of the durability required for multidecade use.

Thermal cycling tests are particularly important for perovskite–silicon tandem system. These tests address the mechanical stress from thermal expansion mismatches between layers, helping to identify risks, such as delamination. Additionally, damp-heat tests that simulate long-term exposure to moisture are vital, as advanced encapsulation techniques struggle to maintain stability under high humidity over extended periods. Tracking *I*–*V* characteristics over time provides invaluable insights into degradation patterns, such as phase segregation and electrode corrosion[328,333]. This approach also helps to identify and manage current mismatches between the perovskite and silicon subcells in tandem solar cells. Accelerated laboratory testing is essential; however, field testing is equally important to evaluate long-term stabilities under varied environmental conditions. Field tests reveal degradation mechanisms, for example, daily thermal cycling and partial shading that may not emerge in controlled environments. These real-world assessments are crucial for bridging the gap between laboratory performance and practical applications.

Economics of perovskite technologies

PSCs represent a potentially disruptive technology in the photovoltaic market, with far-reaching economic implications. Recent market analyses project that the global PSC market could reach US$6.6 billion by 2030, with a compound annual growth rate of 32.4% from 2022 to 2030 (ref. 334). The impact of perovskite technologies extends beyond energy production and into multiple scientific and industrial sectors, for example, in neuromorphic memristors[335] and optical sensor applications[147,336]. In the medical field, perovskites show promise for X-ray detection and radiation therapy monitoring[337]. The unique properties of perovskites make them ideal for integrating into diverse applications, from building and transportation to portable devices and medical implants. This versatility opens new market opportunities in various industries.

Environmental implications

Widespread adoption of PSCs presents a complex environmental landscape with potential benefits and challenges. Life cycle assessments indicate that PSCs could significantly reduce the energy payback time and carbon footprint of solar cells[338]. For example, estimations suggest that perovskite–silicon tandem cells could reduce CO_2 emissions

up to 45% compared with single-junction silicon cells[339]. However, production and deployment of PSCs, particularly those based on lead-containing perovskites, raise concerns with toxicity and ecological impact. Although the quantity of lead in a typical PSC is minimal (~0.8 g m^{-2}), improper disposal or accidental release is an ecological risk[340]. Research into lead-free alternatives, such as tin-based perovskites, is ongoing. Another environmental concern is the use of organic solvents, which can contribute to air pollution and ozone depletion. Advances in solvent-free deposition and green solvent alternatives are promising to mitigate these issues[341]. Non-hazardous solvent systems aim to lower the environmental and health risks of industrial-scale manufacturing. The recyclability of PSCs is an area of active research, with some studies demonstrating up to 90% recovery of perovskite materials[342]. This high recovery rate could make the ecological footprint of perovskite technologies substantially lower than traditional silicon cells, which is difficult to recycle. However, the diversity of PSC architectures makes it hard to develop standardized recycling processes and further research is required in this area. Addressing these environmental challenges is essential for sustainable deployment of PSCs on a large scale. Advances in material science — including developing stable, lead-free perovskites and environmentally benign manufacturing processes — will be crucial. Equally important is to establish a comprehensive regulatory framework to govern the production, use and end-of-life management of PSCs. These efforts, combined with continued improvements in efficiency and stability, will be critical for realizing the full potential of perovskite solar technology while minimizing its environmental impact.

Reproducibility and data deposition

PSCs have gained notoriety for their inconsistent batch-to-batch and lab-to-lab reproducibility, particularly in device performance and stability. This issue affects the entire community, from academic research laboratories to fledgling start-ups and well-established corporations. Achieving consistent and reproducible production is crucial for market viability and practical commercialization. The source of these reproducibility issues is often from hidden variables during fabrication and processing. These elusive factors lead to unintended variations in perovskite composition, defect density and crystal quality. Some are processing-related, such as inconsistent fabrication procedures, fluctuating environmental conditions and varying equipment specifications[60]. Perovskites, with their soft lattice and relatively weak ionic bonds, are inherently sensitive to processing conditions[343]. Their rapid crystallization during solution processing further exacerbates this sensitivity. For instance, the electrostatic interactions between ionic components in perovskite precursors and additives are crucial for regulating crystal growth, but can be easily disrupted by oxygen, humidity and environmental fluctuations[68]. The purity of hygroscopic precursor chemicals is often problematic and independent of the fabrication process. Consequently, the resulting film quality is highly sensitive to precursor chemicals and fabrication conditions, leading to variations in performance and stability.

The unique solution-processed coating method of PSCs, which involves an antisolvent drop during thin film formation, presents another challenge. The timing, volume and type of antisolvent used can impact film quality and introduce variability. Innovative approaches are emerging to address these challenges. For example, robot-controlled fabrication methods enhanced by machine-learning algorithms show promise. These systems provide the precision needed for consistent antisolvent application, whereas machine learning optimizes fabrication parameters in real time, adjusting for environmental fluctuations and material inconsistencies[344,345]. Developing a solvent-free vacuum process could help to improve reproducibility. However, securing reproducibility in the vacuum process requires further optimization of the evaporation system, precursor materials and process parameters.

Considering the reproducibility issues and hidden variables during processing, it is important to fully report all experimental procedures in as much detail as possible. Details such as material supplier, material purity, environmental conditions — temperature, atmosphere, humidity — and equipment specifications are often omitted or not described in sufficient detail in publications. A full video recording demonstrating the fabrication and processing procedures can be helpful for reproducibility. This is not common practice, but most academic journals can support publications with accompanying videos. It is also important to fully report solar cell device and material characterization protocols. Several academic journals require authors to submit a summary report detailing the characterization protocols, including voltage scan conditions, test environment and stability of J–V characteristic, which can influence solar cell characterization. Any unusual behaviour observed during characterization must be declared. Such transparent reporting standards are important to promote reproducibility and repeatability of published works.

Limitations and optimizations

The perovskite active layer has several limitations that impact device performance and long-term stability. A notable challenge comes from the inherent sensitivity of perovskite materials to environmental conditions, such as humidity, oxygen and temperature fluctuations. These factors can lead to uncontrolled crystallization, resulting in defects, non-uniform morphology and phase segregation, which adversely affects device efficiency and stability. The rapid crystallization required during solution processing often introduces inconsistencies in film quality, limiting reproducibility across different batches and laboratories. To address these challenges, researchers are exploring various strategies to optimize perovskite active layer fabrication. Fine-tuning of precursor solutions and solvent engineering are promising to control nucleation and crystal growth, improving uniformity and reducing defects. For instance, mixed solvent systems and carefully selected additives can enhance film quality through better crystallization control[346]. Another promising strategy is to incorporate passivation layers that can mitigate defect sites and improve electronic properties[124]. Advanced deposition techniques, such as vapour-assisted and vacuum-based methods, are being investigated to achieve high-quality perovskite layers with improved film composition and thickness control. These techniques can reduce dependency on solution processing and provide more consistent and scalable fabrication routes[345]. Additionally, using machine-learning algorithms and automated fabrication processes can optimize parameters in real time to produce reproducible and high-performance perovskite active layers. This multifaceted approach, involving material engineering, advanced deposition, automation and machine learning, is crucial for enhancing the efficiency, stability and scalability of PSCs.

Transparent and non-transparent electrodes have similar issues with performance and stability. Metal oxide-based transparent electrodes suffer from high costs and brittleness, limiting their application to flexible devices. Variations in deposition techniques can lead to inconsistencies in film thickness and conductivity, impacting overall device efficiency. For non-transparent electrodes, metal variants are affected by ion migration-driven degradation and limited earth

Glossary

Antisolvent
A solvent used during fabrication to control crystallization and improve the quality of the perovskite layer. The antisolvent is typically immiscible or partially miscible with the perovskite precursor solution and helps induce rapid crystallization, leading to better film formation.

Building-integrated photovoltaics
(BIPV). Photovoltaic materials that can replace conventional building materials in parts of the building envelope such as the roof, skylights or façades.

Charge-selective layers
Materials that facilitate the extraction and transport of specific charge carriers (electrons or holes) to their respective electrodes while blocking the opposite charge carriers. The two main types of charge-selective layers are the electron transport layer and hole transport layer.

Electron transport layer
(ETL). A material that selectively transports electrons from the active layer, where light is absorbed and generates electron–hole pairs, to the electron-collecting electrode, usually the cathode. It also blocks holes from reaching the cathode, preventing recombination of electrons and holes.

External quantum efficiency
The ratio of the number of charge carriers (electrons or holes) generated by the solar cell to the number of incident photons of a given wavelength, expressed as a percentage.

Frank–van der Merwe
Also known as layer-by-layer growth. Describes a thin film growth process in which the adsorbate forms a continuous, smooth layer on the substrate. This mode occurs when the interaction between the adsorbate and substrate is stronger than the interaction between adsorbate atoms.

Goldschmidt tolerance factor
An indicator for the stability and distortion of crystal structures. It was originally only used to describe the perovskite ABO_3 structure, but now tolerance factors are also used for ilmenite.

Hole transport layer
(HTL). A material that selectively transports holes from the active layer to the hole-collecting electrode, usually the anode. It also blocks electrons from reaching the anode, preventing recombination of electrons and holes.

Hysteresis
The presence of different *I*–*V* curves for forward and reverse voltage sweeps, indicating a memory effect in the response of the solar cell to voltage changes.

Incident photon-to-electron conversion efficiency
The percentage of incident photons of a particular wavelength that are converted into electrical charge carriers (electrons or holes) and collected by the solar cell.

Marangoni flow
Also called the Gibbs–Marangoni effect. Describes the mass transfer along an interface between two phases owing to a gradient of the surface tension.

Maximum power point
The point on the *I*–*V* curve where the product of current and voltage (the power) is at its highest. It represents the optimal operating condition in which the solar cell generates the maximum power output under given illumination conditions.

Metal halide perovskite
A class of crystalline materials with the general formula ABX_3, in which A is a monovalent cation, for example, methylammonium, formamidinium or caesium; B is a divalent metal cation, commonly lead or tin; and X is a halide anion, such as chloride, bromide or iodide.

Non-radiative recombination
A process in which electron–hole pairs (excitons) recombine without emitting photons. Instead, the energy is dissipated as heat or transferred to lattice vibrations as phonons.

Open-circuit voltage
The potential difference between the positive and negative terminals of the solar cell when the circuit is not connected to an external load.

Organometal halides
A class of compounds in which an organic group is bonded to a metal atom that is bonded to a halide ion, either chloride, bromide, iodide or fluoride.

Passivation
The process of reducing or eliminating defects and trap states in the perovskite layer or at its interfaces.

Photoactive layer
The central layer responsible for absorbing light and generating charge carriers in the form of electrons and holes. This layer is typically made of metal halide perovskite materials, which have the general formula ABX_3.

Power conversion efficiency
(PCE). The PCE of a solar cell is expressed as the percentage ratio of electrical power produced to optical power impinging on the cell. PCE of a solar cell is calculated from its current–voltage characteristics as follows: $PCE = I_{sc}V_{oc}FF/(E_{tot}A)$; $FF = P_{max}/(I_{sc}V_{oc})$, in which I_{sc} is the short circuit current, V_{oc} is the open circuit voltage, E_{tot} is the total irradiance density, A is the illuminated area, FF is the fill factor and P_{max} is the electrical peak power.

Quantum dot
Semiconductor particles of a few nanometres in size with optical and electronic properties that differ from larger particles owing to quantum mechanical effects.

Stranski–Krastanov
A combined growth mode characterized by initial layer-by-layer growth followed by the formation of islands or clusters. This occurs when the adsorbate–substrate interaction is strong enough to support initial layer growth, but later interaction between adsorbate atoms becomes more favourable, leading to island formation.

Tandem solar cells
Photovoltaic devices that stack multiple layers or cells on top of each other. Each layer is designed to absorb different parts of the solar spectrum. This configuration allows for more efficient use of sunlight compared with single-junction solar cells, as each layer captures and converts different wavelengths.

Volmer–Weber
Also known as island growth. A mode of thin film growth where the adsorbate, the material being deposited, forms discrete islands or clusters on a substrate rather than creating a continuous, smooth film. This occurs when there is strong adsorbate–adsorbate interaction compared with adsorbate–substrate interaction.

abundance. To mitigate these challenges, alternative mechanically pliable, easily processed, cost-effective and environmentally friendly electrodes are being applied to PSCs. Carbon-based materials, such as CNTs and carbon paste, are the most promising. However, they require rigorous optimization and there are relatively fewer carbon material experts working on developing this area. Conducting polymers and metal oxides are being explored for their potential to provide uniform and reproducible films while being scalable and compatible with roll-to-roll manufacturing processes. These materials are promising to address the limitations of traditional electrodes, potentially enhancing the performance and commercial viability of PSCs.

Outlook

There is an optimistic outlook for PSCs, with research looking to tackle current limitations and reach the efficiency, stability and scalability needed for widespread commercial adoption. Recent advances in fabrication techniques and materials engineering will enable PSCs to contribute to the renewable energy landscape. Hybrid deposition techniques are an emerging approach to enhance film quality and uniformity. These techniques combine the simplicity and cost-effectiveness of solution processes with the precision of dry methods. Additive engineering and composition optimization could enhance the morphological and structural properties of perovskite films. Additionally, addressing the toxicity of lead-based perovskites by developing lead-free alternatives, for example, using tin, is crucial for environmental and health safety. Various methodological techniques have a critical role in producing stable lead-free perovskites, which have low reproducibility owing to their instability against humidity and oxygen. To transition from laboratory scale to module will require scalable coating methods, such as slot-die and blade coating, which are well suited for roll-to-roll manufacturing. Developing antisolvent-free processes to modulate solvent evaporation rates is highly important. For instance, slot-die coating enables continuous deposition of perovskite layers on flexible substrates, enabling large-area solar module production. The reproducibility issues when fabricating perovskite active layers are starting to be addressed using robotic systems and artificial intelligence. These systems can dynamically adjust processing conditions and compensate for environmental fluctuations or material inconsistencies, giving more consistent perovskite films. Several key areas demand focused research and development. For example, dry processes are promising for scalable and reproducible fabrication but most research is based on the solution process. Environmental stability is important and there is ongoing work to develop perovskite compositions and encapsulation techniques that resist degradation under environmental stressors. Multilayer barrier films and advanced polymer coatings are being explored as protection for perovskite films and devices, ensuring their stability under real-world conditions. Enhancing the mechanical properties of PSCs is essential to expand applications to flexible and wearable devices. Cost, ion migration-driven degradation and mechanical flexibility are influenced by the electrode materials. Electrodes are moving towards carbon-based alternatives, such as CNTs and carbon paste, which are more flexible and scalable than traditional metals and metal oxides. Further optimization of carbon-based electrodes and hybrid systems could lead to widespread PSC commercialization.

PSCs have numerous compelling advantages over existing photovoltaic technologies. Single-junction PSCs have already surpassed the efficiency of organic solar cells and are approaching inorganic solar cells, such as silicon, CdTe and copper indium gallium selenide cells, typically 15–20% efficiency. In tandem configurations with silicon or a perovskite layer of different chemical compositions, PSCs can exceed 30% efficiency, outperforming commercial thin film photovoltaics. The potential for lower manufacturing costs and simpler fabrication processes contrasts favourably with the energy-intensive production of crystalline silicon and the complex deposition methods required for thin film cells. Unlike rigid silicon cells, perovskites can be fabricated with mechanical flexibility. This is a property shared with organic solar cells, but PSCs have superior efficiency and greater tunability of optical and electronic properties. The versatility of PSCs, characterized by their lightweight nature, mechanical flexibility and semi-transparency, is advantageous for BIPV and portable electronics applications. Although PSCs are a promising next-generation technology, there are challenges with long-term stability and environmental considerations, which are not present for established technologies such as crystalline silicon. Addressing these challenges through innovative fabrication methods, materials design and encapsulation strategies is an important focus of ongoing research efforts.

In conclusion, PSCs are on the cusp of transformative progress. Optimizing manufacturing processes, reducing costs and scaling-up production are crucial for PSCs to compete with established photovoltaic technologies. Their compatibility with roll-to-roll manufacturing offers a path to lower production costs through high-throughput fabrication of large-area modules. Although there are challenges with stability and environmental concerns, ongoing research is rapidly addressing these barriers. The near future is likely to see PSCs transition from laboratory innovations to commercial realities. Breakthroughs are expected in encapsulation techniques and materials engineering to enhance long-term stability. The versatility of PSCs could lead to novel applications beyond traditional solar panels, including BIPV and flexible electronics. Tandem structures combining perovskites with other materials could push solar cell efficiencies beyond current limits. As production scales up, PSCs are expected to be used in diverse markets, from portable electronics to utility-scale solar farms. The potential for low-cost, high-efficiency solar conversion could accelerate the adoption of renewable energy, particularly in developing regions. Overall, PSCs promise to bring major changes to how solar energy is harnessed and used, helping to meet global sustainability goals.

Published online: 16 January 2025

References

1. Kojima, A., Teshima, K., Shirai, Y. & Miyasaka, T. Organometal halide perovskites as visible-light sensitizers for photovoltaic cells. *J. Am. Chem. Soc.* **131**, 6050–6051 (2009).
   To our knowledge, this is the first report on perovskite solar cells.
2. Kim, H.-S. et al. Lead iodide perovskite sensitized all-solid-state submicron thin film mesoscopic solar cell with efficiency exceeding 9%. *Sci. Rep.* **2**, 591 (2012).
   To our knowledge, this article reports the first solid-state perovskite solar cells.
3. Lee, M. M., Teuscher, J., Miyasaka, T., Murakami, T. N. & Snaith, H. J. Efficient hybrid solar cells based on meso-superstructured organometal halide perovskites. *Science* **338**, 643–647 (2012).
4. Liu, S. et al. Buried interface molecular hybrid for inverted perovskite solar cells. *Nature* **632**, 536–542 (2024).
5. Jeon, N. J. et al. Solvent engineering for high-performance inorganic–organic hybrid perovskite solar cells. *Nat. Mater.* **13**, 897–903 (2014).
6. Taylor, A. D. et al. A general approach to high-efficiency perovskite solar cells by any antisolvent. *Nat. Commun.* **12**, 1878 (2021).
7. Han, J. et al. Genetic manipulation of M13 bacteriophage for enhancing the efficiency of virus-inoculated perovskite solar cells with a certified efficiency of 22.3. *Adv. Energy Mater.* https://doi.org/10.1002/aenm.202101221 (2021).
8. Kim, K. et al. Homogeneously miscible fullerene inducing vertical gradient in perovskite thin-film toward highly efficient solar cells. *Adv. Energy Mater.* https://doi.org/10.1002/aenm.202200877 (2022).
9. Kim, K. et al. Liquid-state dithiocarbonate-based polymeric additives with monodispersity rendering perovskite solar cells with exceptionally high certified photocurrent and fill factor. *Adv. Energy Mater.* **13**, 2203742 (2023).

10. Lee, J.-W. et al. A bifunctional Lewis base additive for microscopic homogeneity in perovskite solar cells. *Chem* **3**, 290–302 (2017).
11. Jeon, N. J. et al. Compositional engineering of perovskite materials for high-performance solar cells. *Nature* **517**, 476–480 (2015).
12. McMeekin, D. P. et al. A mixed-cation lead mixed-halide perovskite absorber for tandem solar cells. *Science* **351**, 151–155 (2016).
13. Chen, Q. et al. Planar heterojunction perovskite solar cells via vapor-assisted solution process. *J. Am. Chem. Soc.* **136**, 622–625 (2014).
14. Zuo, L. et al. Polymer-modified halide perovskite films for efficient and stable planar heterojunction solar cells. *Sci. Adv.* **3**, e1700106 (2017).
15. Zuo, L. et al. Enhanced photovoltaic performance of $CH_3NH_3PbI_3$ perovskite solar cells through interfacial engineering using self-assembling monolayer. *J. Am. Chem. Soc.* **137**, 2674–2679 (2015).
16. Degani, M. et al. 23.7% efficient inverted perovskite solar cells by dual interfacial modification. *Sci. Adv.* **7**, eabj7930 (2021).
17. Tao, S. et al. Absolute energy level positions in tin- and lead-based halide perovskites. *Nat. Commun.* **10**, 2560 (2019).
18. Amat, A. et al. Cation-induced band-gap tuning in organohalide perovskites: interplay of spin–orbit coupling and octahedra tilting. *Nano Lett.* **14**, 3608–3616 (2014).
19. Goyal, A. et al. Origin of pronounced nonlinear band gap behavior in lead–tin hybrid perovskite alloys. *Chem. Mater.* **30**, 3920–3928 (2018).
20. Fan, Z., Sun, K. & Wang, J. Perovskites for photovoltaics: a combined review of organic–inorganic halide perovskites and ferroelectric oxide perovskites. *J. Mater. Chem. A Mater.* **3**, 18809–18828 (2015).
21. Park, J. et al. Controlled growth of perovskite layers with volatile alkylammonium chlorides. *Nature* **616**, 724–730 (2023).
22. Liang, Z. et al. Homogenizing out-of-plane cation composition in perovskite solar cells. *Nature* **624**, 557–563 (2023).
23. Lee, J., Seol, D., Cho, A. & Park, N. High-efficiency perovskite solar cells based on the black polymorph of $HC(NH_2)_2PbI_3$. *Adv. Mater.* **26**, 4991–4998 (2014).
24. Kim, J. Y., Lee, J.-W., Jung, H. S. & Shin, H. & Park, N.-G. High-efficiency perovskite solar cells. *Chem. Rev.* **120**, 7867–7918 (2020).
25. Lee, J.-W. et al. Rethinking the A cation in halide perovskites. *Science* **375**, eabj1186 (2022).
26. Li, Z. et al. Stabilizing perovskite structures by tuning tolerance factor: formation of formamidinium and cesium lead iodide solid-state alloys. *Chem. Mater.* **28**, 284–292 (2016).
27. Qiu, Z., Li, N., Huang, Z., Chen, Q. & Zhou, H. Recent advances in improving phase stability of perovskite solar cells. *Small Methods* https://doi.org/10.1002/smtd.201900877 (2020).
28. Chen, T. et al. Entropy-driven structural transition and kinetic trapping in formamidinium lead iodide perovskite. *Sci. Adv.* **2**, e1601650 (2016).
29. Bechtel, J. S. & Van der Ven, A. Octahedral tilting instabilities in inorganic halide perovskites. *Phys. Rev. Mater.* **2**, 025401 (2018).
30. Hoke, E. T. et al. Reversible photo-induced trap formation in mixed-halide hybrid perovskites for photovoltaics. *Chem. Sci.* **6**, 613–617 (2015).
31. Yoo, J. J. et al. Efficient perovskite solar cells via improved carrier management. *Nature* **590**, 587–593 (2021).
32. Jang, Y.-W. et al. Intact 2D/3D halide junction perovskite solar cells via solid-phase in-plane growth. *Nat. Energy* **6**, 63–71 (2021).
33. Jiang, Q. et al. Surface passivation of perovskite film for efficient solar cells. *Nat. Photon.* **13**, 460–466 (2019).
This article is a pioneering work that shows the potential of surface passivation, now widely used in state-of-the-art perovskite solar cells.
34. Li, X. et al. Constructing heterojunctions by surface sulfidation for efficient inverted perovskite solar cells. *Science* **375**, 434–437 (2022).
35. Tan, Q. et al. Inverted perovskite solar cells using dimethylacridine-based dopants. *Nature* **620**, 545–551 (2023).
36. Zhang, S. et al. Minimizing buried interfacial defects for efficient inverted perovskite solar cells. *Science* **380**, 404–409 (2023).
37. Peng, W. et al. Reducing nonradiative recombination in perovskite solar cells with a porous insulator contact. *Science* **379**, 683–690 (2023).
38. Wu, X. et al. Backbone engineering enables highly efficient polymer hole-transporting materials for inverted perovskite solar cells. *Adv. Mater.* **35**, e2208431 (2023).
39. Jiang, Q. et al. Surface reaction for efficient and stable inverted perovskite solar cells. *Nature* **611**, 278–283 (2022).
40. Li, Z. et al. Organometallic-functionalized interfaces for highly efficient inverted perovskite solar cells. *Science* **376**, 416–420 (2022).
41. Lee, J. et al. Formamidinium and cesium hybridization for photo- and moisture-stable perovskite solar cell. *Adv. Energy Mater.* https://doi.org/10.1002/aenm.201501310 (2015).
This article reports a strategy for stabilizing formamidinium perovskites, widely used in state-of-the-art perovskite solar cells.
42. Liu, X. et al. Stabilization of photoactive phases for perovskite photovoltaics. *Nat. Rev. Chem.* **7**, 462–479 (2023).
43. Isikgor, F. H. et al. Concurrent cationic and anionic perovskite defect passivation enables 27.4% perovskite/silicon tandems with suppression of halide segregation. *Joule* **5**, 1566–1586 (2021).
44. Li, N. et al. Microscopic degradation in formamidinium–cesium lead iodide perovskite solar cells under operational stressors. *Joule* **4**, 1743–1758 (2020).
45. Jeong, M. J. et al. Boosting radiation of stacked halide layer for perovskite solar cells with efficiency over 25%. *Joule* **7**, 112–127 (2023).
46. Kim, M. et al. Conformal quantum dot–SnO_2 layers as electron transporters for efficient perovskite solar cells. *Science* **375**, 302–306 (2022).
47. Min, H. et al. Perovskite solar cells with atomically coherent interlayers on SnO_2 electrodes. *Nature* **598**, 444–450 (2021).
48. Jeong, J. et al. Pseudo-halide anion engineering for α-$FAPbI_3$ perovskite solar cells. *Nature* **592**, 381–385 (2021).
49. Kim, M. et al. Methylammonium chloride induces intermediate phase stabilization for efficient perovskite solar cells. *Joule* **3**, 2179–2192 (2019).
50. Lee, J.-W. et al. 2D perovskite stabilized phase-pure formamidinium perovskite solar cells. *Nat. Commun.* **9**, 3021 (2018).
51. Sidhik, S. et al. Two-dimensional perovskite templates for durable, efficient formamidinium perovskite solar cells. *Science* **384**, 1227–1235 (2024).
52. Lee, J.-W. et al. Solid-phase hetero epitaxial growth of α-phase formamidinium perovskite. *Nat. Commun.* **11**, 5514 (2020).
53. Ahn, N. et al. Highly reproducible perovskite solar cells with average efficiency of 18.3% and best efficiency of 19.7% fabricated via Lewis base adduct of lead(II) iodide. *J. Am. Chem. Soc.* **137**, 8696–8699 (2015).
This article reports a methodology for depositing uniform perovskite films, widely used in perovskite solar cells.
54. Lee, J.-W., Kim, H.-S. & Park, N.-G. Lewis acid–base adduct approach for high efficiency perovskite solar cells. *Acc. Chem. Res.* **49**, 311–319 (2016).
55. Hamill, J. C., Schwartz, J. & Loo, Y.-L. Influence of solvent coordination on hybrid organic–inorganic perovskite formation. *ACS Energy Lett.* **3**, 92–97 (2018).
56. Lee, J.-W. et al. Tuning molecular interactions for highly reproducible and efficient formamidinium perovskite solar cells via adduct approach. *J. Am. Chem. Soc.* **140**, 6317–6324 (2018).
57. Wu, T. et al. Solvent engineering for high-quality perovskite solar cell with an efficiency approaching 20%. *J. Power Sources* **365**, 1–6 (2017).
58. Lee, C. M. et al. Impact of ternary solvent on the grain size and defects of perovskite layer to realize a stable morphology for efficient inverted solar cells. *Sol. RRL* https://doi.org/10.1002/solr.202300604 (2023).
59. Bautista-Quijano, J. R., Telschow, O., Paulus, F. & Vaynzof, Y. Solvent–antisolvent interactions in metal halide perovskites. *Chem. Commun.* **59**, 10588–10603 (2023).
60. Goetz, K. P. & Vaynzof, Y. The challenge of making the same device twice in perovskite photovoltaics. *ACS Energy Lett.* **7**, 1750–1757 (2022).
61. Ahn, N., Kang, S. M., Lee, J.-W., Choi, M. & Park, N.-G. Thermodynamic regulation of $CH_3NH_3PbI_3$ crystal growth and its effect on photovoltaic performance of perovskite solar cells. *J. Mater. Chem. A Mater.* **3**, 19901–19906 (2015).
62. Yang, W. S. et al. High-performance photovoltaic perovskite layers fabricated through intramolecular exchange. *Science* **348**, 1234–1237 (2015).
63. Xie, L. et al. Efficient and stable low-bandgap perovskite solar cells enabled by a $CsPbBr_3$-cluster assisted bottom-up crystallization approach. *J. Am. Chem. Soc.* **141**, 20537–20546 (2019).
64. Zhao, Y. et al. Inactive $(PbI_2)_2RbCl$ stabilizes perovskite films for efficient solar cells. *Science* **377**, 531–534 (2022).
65. Swarnkar, A. et al. Quantum dot-induced phase stabilization of α-$CsPbI_3$ perovskite for high-efficiency photovoltaics. *Science* **354**, 92–95 (2016).
This article is one of the first pioneering works demonstrating the potential of perovskite quantum dot solar cells.
66. Saliba, M. et al. Incorporation of rubidium cations into perovskite solar cells improves photovoltaic performance. *Science* **354**, 206–209 (2016).
67. Tan, S. et al. Steric impediment of ion migration contributes to improved operational stability of perovskite solar cells. *Adv. Mater.* **2**, e1906995 (2020).
68. Park, K. et al. Atmospheric humidity underlies irreproducibility of formamidinium lead iodide perovskites. *Adv. Mater.* **36**, e2307265 (2024).
69. Tan, S. et al. Shallow iodine defects accelerate the degradation of α-phase formamidinium perovskite. *Joule* **4**, 2426–2442 (2020).
70. Tan, S. et al. Stability-limiting heterointerfaces of perovskite photovoltaics. *Nature* **605**, 268–273 (2022).
71. Huang, T., Tan, S. & Yang, Y. Material, phase, and interface stability of photovoltaic perovskite: a perspective. *J. Phys. Chem. C* **125**, 19088–19096 (2021).
72. Han, T. et al. Interface and defect engineering for metal halide perovskite optoelectronic devices. *Adv. Mater.* **31**, e1803515 (2019).
73. Tan, S. et al. Surface reconstruction of halide perovskites during post-treatment. *J. Am. Chem. Soc.* **143**, 6781–6786 (2021).
74. Park, S. M. et al. Engineering ligand reactivity enables high-temperature operation of stable perovskite solar cells. *Science* **381**, 209–215 (2023).
75. Azmi, R. et al. Damp heat-stable perovskite solar cells with tailored-dimensionality 2D/3D heterojunctions. *Science* **376**, 73–77 (2022).
76. Zhou, P. et al. Ultrasonic spray-coating of large-scale TiO_2 compact layer for efficient flexible perovskite solar cells. *Micromachines* **8**, 55 (2017).
77. Das, S. et al. High-performance flexible perovskite solar cells by using a combination of ultrasonic spray-coating and low thermal budget photonic curing. *ACS Photon.* **2**, 680–686 (2015).
78. Wang, Z. et al. Rational interface design and morphology control for blade-coating efficient flexible perovskite solar cells with a record fill factor of 81%. *Adv. Funct. Mater.* **30**, 2001240 (2020).

79. Wilk, B. et al. Green solvent-based perovskite precursor development for ink-jet printed flexible solar cells. *ACS Sustain. Chem. Eng.* **9**, 3920–3930 (2021).
80. Xing, Z. et al. A highly tolerant printing for scalable and flexible perovskite solar cells. *Adv. Funct. Mater*. https://doi.org/10.1002/adfm.202107726 (2021).
81. Li, H. et al. Fully roll-to-roll processed efficient perovskite solar cells via precise control on the morphology of PbI_2:CsI layer. *Nanomicro Lett.* **14**, 79 (2022).
82. Krechetnikov, R. & Homsy, G. M. Surfactant effects in the Landau–Levich problem. *J. Fluid Mech.* **559**, 429 (2006).
83. Parvazian, E., Abdollah-zadeh, A., Dehghani, M. & Taghavinia, N. Photovoltaic performance improvement in vacuum-assisted meniscus printed triple-cation mixed-halide perovskite films by surfactant engineering. *ACS Appl. Energy Mater.* **2**, 6209–6217 (2019).
84. Li, C. et al. Monoammonium porphyrin for blade-coating stable large-area perovskite solar cells with >18% efficiency. *J. Am. Chem. Soc.* **141**, 6345–6351 (2019).
85. Lee, S. & Nam, J. Analysis of slot coating flow under tilted die. *AIChE J.* **61**, 1745–1758 (2015).
86. Krebs, F. C. Fabrication and processing of polymer solar cells: a review of printing and coating techniques. *Sol. Energy Mater. Sol. Cell* **93**, 394–412 (2009).
87. Cotella, G. et al. One-step deposition by slot-die coating of mixed lead halide perovskite for photovoltaic applications. *Sol. Energy Mater. Sol. Cell* **159**, 362–369 (2017).
88. Heo, J. H., Lee, M. H., Jang, M. H. & Im, S. H. Highly efficient $CH_3NH_3PbI_{3-x}Cl_x$ mixed halide perovskite solar cells prepared by re-dissolution and crystal grain growth via spray coating. *J. Mater. Chem. A Mater.* **4**, 17636–17642 (2016).
89. Yu, Y.-T. et al. One-step spray-coated all-inorganic $CsPbI_2Br$ perovskite solar cells. *ACS Appl. Energy Mater.* **4**, 5466–5474 (2021).
90. Bishop, J. E., Read, C. D., Smith, J. A., Routledge, T. J. & Lidzey, D. G. Fully spray-coated triple-cation perovskite solar cells. *Sci. Rep.* **10**, 6610 (2020).
91. Barrows, A. T. et al. Efficient planar heterojunction mixed-halide perovskite solar cells deposited via spray-deposition. *Energy Environ. Sci.* **7**, 2944–2950 (2014).
92. Zhang, L. et al. Ambient inkjet-printed high-efficiency perovskite solar cells: manipulating the spreading and crystallization behaviors of picoliter perovskite droplets. *Sol. RRL* https://doi.org/10.1002/solr.202100106 (2021).
93. Duan, Y., Huang, Y., Yin, Z., Bu, N. & Dong, W. Non-wrinkled, highly stretchable piezoelectric devices by electrohydrodynamic direct-writing. *Nanoscale* **6**, 3289 (2014).
94. Fromm, J. E. Numerical calculation of the fluid dynamics of drop-on-demand jets. *IBM J. Res. Dev.* **28**, 322–333 (1984).
95. Vaynzof, Y. The future of perovskite photovoltaics — thermal evaporation or solution processing? *Adv. Energy Mater*. https://doi.org/10.1002/aenm.202003073 (2020).
96. Ji, R. et al. Perovskite phase heterojunction solar cells. *Nat. Energy* **7**, 1170–1179 (2022).
97. Kottokkaran, R., Gaonkar, H. A., Abbas, H. A., Noack, M. & Dalal, V. Performance and stability of co-evaporated vapor deposited perovskite solar cells. *J. Mater. Sci. Mater. Electron.* **30**, 5487–5494 (2019).
98. Wang, S. et al. Smooth perovskite thin films and efficient perovskite solar cells prepared by the hybrid deposition method. *J. Mater. Chem. A Mater.* **3**, 14631–14641 (2015).
99. Kim, B.-S., Choi, M.-H., Choi, M.-S. & Kim, J.-J. Composition-controlled organometal halide perovskite via CH_3NH_3I pressure in a vacuum co-deposition process. *J. Mater. Chem. A Mater.* **4**, 5663–5668 (2016).
100. Teuscher, J., Ulianov, A., Müntener, O., Grätzel, M. & Tétreault, N. Control and study of the stoichiometry in evaporated perovskite solar cells. *ChemSusChem* **8**, 3847–3852 (2015).
101. Kim, B.-S., Gil-Escrig, L., Sessolo, M. & Bolink, H. J. Deposition kinetics and compositional control of vacuum-processed $CH_3NH_3PbI_3$ perovskite. *J. Phys. Chem. Lett.* **11**, 6852–6859 (2020).
102. Kroll, M. et al. Insights into the evaporation behaviour of FAI: material degradation and consequences for perovskite solar cells. *Sustain. Energy Fuels* **6**, 3230–3239 (2022).
103. Lee, J., Kim, B. S., Park, J., Lee, J. & Kim, K. Opportunities and challenges for perovskite solar cells based on vacuum thermal evaporation. *Adv. Mater. Technol.* **8**, 2200928 (2023).
104. Zhou, J. et al. Highly efficient and stable perovskite solar cells via a multifunctional hole transporting material. *Joule* **8**, 1691–1706 (2024).
105. Li, H. et al. Sequential vacuum-evaporated perovskite solar cells with more than 24% efficiency. *Sci. Adv.* **8**, eabo7422 (2022).
106. Zhang, W. et al. Enhanced optoelectronic quality of perovskite thin films with hypophosphorous acid for planar heterojunction solar cells. *Nat. Commun.* **6**, 10030 (2015).
107. Zhao, Y. & Zhu, K. CH_3NH_3Cl-assisted one-step solution growth of $CH_3NH_3PbI_3$: structure, charge-carrier dynamics, and photovoltaic properties of perovskite solar cells. *J. Phys. Chem. C* **118**, 9412–9418 (2014).
108. Soltanpoor, W. et al. Hybrid vapor-solution sequentially deposited mixed-halide perovskite solar cells. *ACS Appl. Energy Mater.* **3**, 8257–8265 (2020).
109. Wang, S. et al. Over 24% efficient MA-free $Cs_xFA_{1-x}PbX_3$ perovskite solar cells. *Joule* **6**, 1344–1356 (2022).
110. Aqoma, H. et al. Alkyl ammonium iodide-based ligand exchange strategy for high-efficiency organic-cation perovskite quantum dot solar cells. *Nat. Energy* **9**, 324–332 (2024).
111. Protesescu, L. et al. Nanocrystals of cesium lead halide perovskites (CsPbX3, X=Cl, Br, and I): novel optoelectronic materials showing bright emission with wide color gamut. *Nano Lett.* **15**, 3692–3696 (2015).
112. Zhang, F. et al. Brightly luminescent and color-tunable colloidal $CH_3NH_3PbX_3$ (X=Br, I, Cl) quantum dots: potential alternatives for display technology. *ACS Nano* **9**, 4533–4542 (2015).
113. Lignos, I. et al. Synthesis of cesium lead halide perovskite nanocrystals in a droplet-based microfluidic platform: fast parametric space mapping. *Nano Lett.* **16**, 1869–1877 (2016).
114. Wheeler, L. M. et al. Targeted ligand-exchange chemistry on cesium lead halide perovskite quantum dots for high-efficiency photovoltaics. *J. Am. Chem. Soc.* **140**, 10504–10513 (2018).
115. Xue, J. et al. Surface ligand management for stable $FAPbI_3$ perovskite quantum dot solar cells. *Joule* **2**, 1866–1878 (2018).
116. Akkerman, Q. A. et al. Tuning the optical properties of cesium lead halide perovskite nanocrystals by anion exchange reactions. *J. Am. Chem. Soc.* **137**, 10276–10281 (2015).
117. Shi, J. et al. In situ ligand bonding management of $CsPbI_3$ perovskite quantum dots enables high-performance photovoltaics and red light-emitting diodes. *Angew. Chem. Int. Ed.* **59**, 22230–22237 (2020).
118. Bi, C., Kershaw, S. V., Rogach, A. L. & Tian, J. Improved stability and photodetector performance of $CsPbI_3$ perovskite quantum dots by ligand exchange with aminoethanethiol. *Adv. Funct. Mater*. https://doi.org/10.1002/adfm.201902446 (2019).
119. Sanehira, E. M. et al. Enhanced mobility $CsPb_3$ quantum dot arrays for record-efficiency, high-voltage photovoltaic cells. *Sci. Adv.* **3**, eaao4204 (2017).
120. Flora, G., Gupta, D. & Tiwari, A. Toxicity of lead: a review with recent updates. *Interdiscip. Toxicol.* **5**, 47–58 (2012).
121. Babayigit, A., Ethirajan, A., Muller, M. & Conings, B. Toxicity of organometal halide perovskite solar cells. *Nat. Mater.* **15**, 247–251 (2016).
122. Chen, S. et al. Preventing lead leakage with built-in resin layers for sustainable perovskite solar cells. *Nat. Sustain.* **4**, 636–643 (2021).
123. Wu, P., Wang, S., Li, X. & Zhang, F. Beyond efficiency fever: preventing lead leakage for perovskite solar cells. *Matter* **5**, 1137–1161 (2022).
124. Liang, Y. et al. Lead leakage preventable fullerene–porphyrin dyad for efficient and stable perovskite solar cells. *Adv. Funct. Mater.* **32**, 2110139 (2022).
125. Jiang, X. et al. Ultra-high open-circuit voltage of tin perovskite solar cells via an electron transporting layer design. *Nat. Commun.* **11**, 1245 (2020).
126. López-Fernández, I. et al. Lead-free halide perovskite materials and optoelectronic devices: progress and prospective. *Adv. Funct. Mater*. https://doi.org/10.1002/adfm.202307896 (2024).
127. Jeon, I. et al. Environmentally compatible lead-free perovskite solar cells and their potential as light harvesters in energy storage systems. *Nanomaterials* **11**, 2066 (2021).
128. Yu, B. et al. Heterogeneous 2D/3D tin-halides perovskite solar cells with certified conversion efficiency breaking 14%. *Adv. Mater*. https://doi.org/10.1002/adma.202102055 (2021).
129. Xiao, Z., Song, Z. & Yan, Y. From lead halide perovskites to lead-free metal halide perovskites and perovskite derivatives. *Adv. Mater.* **31**, e1803792 (2019).
130. Jokar, E. et al. Mixing of azetidinium in formamidinium tin triiodide perovskite solar cells for enhanced photovoltaic performance and high stability in air. *ChemSusChem* **14**, 4415–4421 (2021).
131. Kuan, C.-H. et al. Additive engineering with triple cations and bifunctional sulfamic acid for tin perovskite solar cells attaining a PCE value of 12.5% without hysteresis. *ACS Energy Lett.* **7**, 4436–4442 (2022).
132. Jokar, E., Chien, C., Tsai, C., Fathi, A. & Diau, E. W. Robust tin-based perovskite solar cells with hybrid organic cations to attain efficiency approaching 10%. *Adv. Mater*. https://doi.org/10.1002/adma.201804835 (2019).
133. Jokar, E. et al. Slow surface passivation and crystal relaxation with additives to improve device performance and durability for tin-based perovskite solar cells. *Energy Environ. Sci.* **11**, 2353–2362 (2018).
This article is one of the earliest works contributing to efficiency and stability improvements in lead-free perovskite solar cells.
134. Shahbazi, S., Li, M.-Y., Fathi, A. & Diau, E. W.-G. Realizing a cosolvent system for stable tin-based perovskite solar cells using a two-step deposition approach. *ACS Energy Lett.* **5**, 2508–2511 (2020).
135. Kuan, C.-H., Ko, Y.-A. & Wei-Guang Diau, E. Surface and interfacial passivations for $FASnI_3$ solar cells with co-cations. *ACS Energy Lett.* **8**, 2423–2425 (2023).
136. Jokar, E. et al. Enhanced performance and stability of 3D/2D tin perovskite solar cells fabricated with a sequential solution deposition. *ACS Energy Lett.* **6**, 485–492 (2021).
137. Kuan, C.-H. et al. How can a hydrophobic polymer PTAA serve as a hole-transport layer for an inverted tin perovskite solar cell? *Chem. Eng. J.* **450**, 138037 (2022).
138. Kuan, C. et al. Dopant-free pyrrolopyrrole-based (PPr) polymeric hole-transporting materials for efficient tin-based perovskite solar cells with stability over 6000 h. *Adv. Mater.* **35**, e2300681 (2023).
139. Balasaravanan, R. et al. Triphenylamine (TPA)-functionalized structural isomeric polythiophenes as dopant free hole-transporting materials for tin perovskite solar cells. *Adv. Energy Mater*. https://doi.org/10.1002/aenm.202302047 (2023).
140. Afraj, S. N. et al. Quinoxaline-based X-shaped sensitizers as self-assembled monolayer for tin perovskite solar cells. *Adv. Funct. Mater*. https://doi.org/10.1002/adfm.202213939 (2023).
141. Song, D., Narra, S., Li, M.-Y., Lin, J.-S. & Diau, E. W.-G. Interfacial engineering with a hole-selective self-assembled monolayer for tin perovskite solar cells via a two-step fabrication. *ACS Energy Lett.* **6**, 4179–4186 (2021).
142. Abid, A., Rajamanickam, P. & Wei-Guang Diau, E. Design of a simple bifunctional system as a self-assembled monolayer (SAM) for inverted tin-based perovskite solar cells. *Chem. Eng. J.* **477**, 146755 (2023).
143. Wu, T. et al. Lead-free tin perovskite solar cells. *Joule* **5**, 863–886 (2021).
144. Song, T.-B. et al. Importance of reducing vapor atmosphere in the fabrication of tin-based perovskite solar cells. *J. Am. Chem. Soc.* **139**, 836–842 (2017).

145. Macdonald, T. J., Lanzetta, L., Liang, X., Ding, D. & Haque, S. A. Engineering stable lead-free tin halide perovskite solar cells: lessons from materials chemistry. *Adv. Mater.* **35**, e2206684 (2023).
146. Kim, G. et al. Sustainable and environmentally viable perovskite solar cells. *EcoMat* https://doi.org/10.1002/eom2.12319 (2023).
147. Jokar, E., Cai, L., Han, J., Nacpil, E. J. C. & Jeon, I. Emerging opportunities in lead-free and lead–tin perovskites for environmentally viable photodetector applications. *Chem. Mater.* **35**, 3404–3426 (2023).
148. Byranvand, M. M., Zuo, W., Imani, R., Pazoki, M. & Saliba, M. Tin-based halide perovskite materials: properties and applications. *Chem. Sci.* **13**, 6766–6781 (2022).
149. Aktas, E. et al. Challenges and strategies toward long-term stability of lead-free tin-based perovskite solar cells. *Commun. Mater.* **3**, 104 (2022).
150. Slavney, A. H., Hu, T., Lindenberg, A. M. & Karunadasa, H. I. A bismuth-halide double perovskite with long carrier recombination lifetime for photovoltaic applications. *J. Am. Chem. Soc.* **138**, 2138–2141 (2016).
151. Chu, L. et al. Lead-free halide double perovskite materials: a new superstar toward green and stable optoelectronic applications. *Nanomicro Lett.* **11**, 16 (2019).
152. McClure, E. T., Ball, M. R., Windl, W. & Woodward, P. M. Cs_2AgBiX_6 (X=Br, Cl): new visible light absorbing, lead-free halide perovskite semiconductors. *Chem. Mater.* **28**, 1348–1354 (2016).
153. Khalfin, S. & Bekenstein, Y. Advances in lead-free double perovskite nanocrystals, engineering band-gaps and enhancing stability through composition tunability. *Nanoscale* **11**, 8665–8679 (2019).
154. Diao, X. et al. High-throughput screening of stable and efficient double inorganic halide perovskite materials by DFT. *Sci. Rep.* **12**, 12633 (2022).
155. Tong, J. et al. Carrier lifetimes of >1 μs in Sn-Pb perovskites enable efficient all-perovskite tandem solar cells. *Science* **364**, 475–479 (2019).
156. Lin, R. et al. Monolithic all-perovskite tandem solar cells with 24.8% efficiency exploiting comproportionation to suppress Sn(ii) oxidation in precursor ink. *Nat. Energy* **4**, 864–873 (2019).
157. Xu, J. et al. Triple-halide wide-band gap perovskites with suppressed phase segregation for efficient tandems. *Science* **367**, 1097–1104 (2020).
158. Abdollahi Nejand, B. et al. Scalable two-terminal all-perovskite tandem solar modules with a 19.1% efficiency. *Nat. Energy* **7**, 620–630 (2022).
159. Ghosh, S., Shankar, H. & Kar, P. Recent developments of lead-free halide double perovskites: a new superstar in the optoelectronic field. *Mater. Adv.* **3**, 3742–3765 (2022).
160. Ahn, N. et al. Carbon-sandwiched perovskite solar cell. *J. Mater. Chem. A Mater.* **6**, 1382–1389 (2018).
161. Kogo, A., Sanehira, Y., Numata, Y., Ikegami, M. & Miyasaka, T. Amorphous metal oxide blocking layers for highly efficient low-temperature brookite TiO_2-based perovskite solar cells. *ACS Appl. Mater. Interfaces* **10**, 2224–2229 (2018).
162. Zhou, H. et al. Interface engineering of highly efficient perovskite solar cells. *Science* **345**, 542–546 (2014).
163. Jiang, Q., Zhang, X. & You, J. SnO_2: a wonderful electron transport layer for perovskite solar cells. *Small* **14**, e1801154 (2018).
164. Hu, W., Yang, S. & Yang, S. Surface modification of TiO_2 for perovskite solar cells. *Trends Chem.* **2**, 148–162 (2020).
165. Park, M. et al. Low-temperature solution-processed Li-doped SnO_2 as an effective electron transporting layer for high-performance flexible and wearable perovskite solar cells. *Nano Energy* **26**, 208–215 (2016).
166. Jiang, Q. et al. Enhanced electron extraction using SnO_2 for high-efficiency planar-structure $HC(NH_2)_2PbI_3$-based perovskite solar cells. *Nat. Energy* **2**, 16177 (2016).
167. Wang, D., He, T., Li, S., Jiang, Y. & Yuan, M. Li-doped chemical bath deposited SnO_2 enables efficient perovskite photovoltaics. *ACS Appl. Energy Mater.* **5**, 5340–5347 (2022).
168. Long, W., He, A., Xie, S., Yang, X. & Wu, L. Prospect of SnO_2 electron transport layer deposited by ultrasonic spraying. *Energies* **15**, 3211 (2022).
169. Thote, A. et al. High-working-pressure sputtering of ZnO for stable and efficient perovskite solar cells. *ACS Appl. Electron. Mater.* **1**, 389–396 (2019).
170. Ciro, J. et al. Self-functionalization behind a solution-processed NiO_x film used as hole transporting layer for efficient perovskite solar cells. *ACS Appl. Mater. Interfaces* **9**, 12348–12354 (2017).
171. Liu, M.-H. et al. p-type Li, Cu-codoped NiO_x hole-transporting layer for efficient planar perovskite solar cells. *Opt. Express* **24**, A1349 (2016).
172. Yin, X., Guo, Y., Xie, H., Que, W. & Kong, L. B. Nickel oxide as efficient hole transport materials for perovskite solar cells. *Solar RRL* https://doi.org/10.1002/solr.201900001 (2019).
173. Zhu, Z. et al. High-performance hole-extraction layer of sol–gel-processed NiO nanocrystals for inverted planar perovskite solar cells. *Angew. Chem. Int. Ed.* **53**, 12571–12575 (2014).
174. Liu, Z. et al. High-performance planar perovskite solar cells using low temperature, solution–combustion-based nickel oxide hole transporting layer with efficiency exceeding 20%. *Adv. Energy Mater.* **8**, 1703432 (2018).
175. Ye, F. et al. Soft-cover deposition of scaling-up uniform perovskite thin films for high cost-performance solar cells. *Energy Environ. Sci.* **9**, 2295–2301 (2016).
176. Sun, J. et al. Inverted perovskite solar cells with high fill-factors featuring chemical bath deposited mesoporous NiO hole transporting layers. *Nano Energy* **49**, 163–171 (2018).
177. Park, I. J. et al. Highly efficient and uniform 1 cm^2 perovskite solar cells with an electrochemically deposited NiO_x hole-extraction layer. *ChemSusChem* **10**, 2660–2667 (2017).
178. Seo, S. et al. An ultra-thin, un-doped NiO hole transporting layer of highly efficient (16.4%) organic–inorganic hybrid perovskite solar cells. *Nanoscale* **8**, 11403–11412 (2016).
179. Zheng, X. et al. Interface modification of sputtered NiO_x as the hole-transporting layer for efficient inverted planar perovskite solar cells. *J. Mater. Chem. C Mater.* **8**, 1972–1980 (2020).
180. Qiu, Z. et al. Enhanced physical properties of pulsed laser deposited NiO films via annealing and lithium doping for improving perovskite solar cell efficiency. *J. Mater. Chem. C. Mater,* **5**, 7084–7094 (2017).
181. Abzieher, T. et al. Electron-beam-evaporated nickel oxide hole transport layers for perovskite-based photovoltaics. *Adv. Energy Mater.* **9**, 1802995 (2019).
182. Guo, R. et al. Significant performance enhancement of all-inorganic $CsPbBr_3$ perovskite solar cells enabled by Nb-doped SnO_2 as effective electron transport layer. *Energy Environ. Mater.* **4**, 671–680 (2021).
183. Lee, Y. et al. Efficient planar perovskite solar cells using passivated tin oxide as an electron transport layer. *Adv. Sci.* **5**, 1800130 (2018).
184. George, S. M. Atomic layer deposition: an overview. *Chem. Rev.* **110**, 111–131 (2010).
185. Profijt, H. B., Potts, S. E., van de Sanden, M. C. M. & Kessels, W. M. M. Plasma-assisted atomic layer deposition: basics, opportunities, and challenges. *J. Vac. Sci. Technol. A Vac. Surf. Films* **29**, 050801 (2011).
186. Zardetto, V. et al. Opportunities of atomic layer deposition for perovskite solar cells. *ECS Trans.* **69**, 15–22 (2015).
187. Zardetto, V. et al. Atomic layer deposition for perovskite solar cells: research status, opportunities and challenges. *Sustain. Energy Fuels* **1**, 30–55 (2017).
188. Du, M. et al. Surface redox engineering of vacuum-deposited NiO_x for top-performance perovskite solar cells and modules. *Joule* **6**, 1931–1943 (2022).
189. Son, M.-K. et al. A copper nickel mixed oxide hole selective layer for Au-free transparent cuprous oxide photocathodes. *Energy Environ. Sci.* **10**, 912–918 (2017).
190. Kim, J. H. et al. High-performance and environmentally stable planar heterojunction perovskite solar cells based on a solution-processed copper-doped nickel oxide hole-transporting layer. *Adv. Mater.* **27**, 695–701 (2015).
191. Chen, W. et al. Cesium doped NiO_x as an efficient hole extraction layer for inverted planar perovskite solar cells. *Adv. Energy Mater.* **7**, 1700722 (2017).
192. Ru, P. et al. High electron affinity enables fast hole extraction for efficient flexible inverted perovskite solar cells. *Adv. Energy Mater*. https://doi.org/10.1002/aenm.201903487 (2020).
193. Li, C. et al. Efficient inverted perovskite solar cells with a fill factor over 86% via surface modification of the nickel oxide hole contact. *Adv. Funct. Mater*. https://doi.org/10.1002/adfm.202214774 (2023).
194. Eggers, H. et al. Inkjet-printed micrometer-thick perovskite solar cells with large columnar grains. *Adv. Energy Mater.* **10**, 1903184 (2020).
195. Kavan, L., Steier, L. & Grätzel, M. Ultrathin buffer layers of SnO_2 by atomic layer deposition: perfect blocking function and thermal stability. *J. Phys. Chem. C* **121**, 342–350 (2017).
196. Jeong, S., Seo, S., Park, H. & Shin, H. Atomic layer deposition of a SnO_2 electron-transporting layer for planar perovskite solar cells with a power conversion efficiency of 18.3%. *Chem. Commun.* **55**, 2433–2436 (2019).
197. Yang, G. et al. Effective carrier-concentration tuning of SnO_2 quantum dot electron-selective layers for high-performance planar perovskite solar cells. *Adv. Mater*. https://doi.org/10.1002/adma.201706023 (2018).
198. Qiu, L. et al. Scalable fabrication of stable high efficiency perovskite solar cells and modules utilizing room temperature sputtered SnO_2 electron transport layer. *Adv. Funct. Mater*. https://doi.org/10.1002/adfm.201806779 (2019).
199. Ke, W. et al. Low-temperature solution-processed tin oxide as an alternative electron transporting layer for efficient perovskite solar cells. *J. Am. Chem. Soc.* **137**, 6730–6733 (2015).
200. Al-Ashouri, A. et al. Monolithic perovskite/silicon tandem solar cell with >29% efficiency by enhanced hole extraction. *Science* **370**, 1300–1309 (2020).
201. Correa Baena, J. P. et al. Highly efficient planar perovskite solar cells through band alignment engineering. *Energy Environ. Sci.* **8**, 2928–2934 (2015).
202. Hill, R. B. M. et al. Phosphonic acid modification of the electron selective contact: interfacial effects in perovskite solar cells. *ACS Appl. Energy Mater.* **2**, 2402–2408 (2019).
203. Ren, N. et al. 50 °C low-temperature ALD SnO_2 driven by H_2O_2 for efficient perovskite and perovskite/silicon tandem solar cells. *Appl. Phys. Lett.* **121**, 033502 (2022).
204. Lee, S.-U., Park, H., Shin, H. & Park, N.-G. Atomic layer deposition of SnO_2 using hydrogen peroxide improves the efficiency and stability of perovskite solar cells. *Nanoscale* **15**, 5044–5052 (2023).
205. Scalon, L., Vaynzof, Y., Nogueira, A. F. & Oliveira, C. C. How organic chemistry can affect perovskite photovoltaics. *Cell Rep. Phys. Sci.* **4**, 101358 (2023).
206. Saragi, T. P. I., Spehr, T., Siebert, A., Fuhrmann-Lieker, T. & Salbeck, J. Spiro compounds for organic optoelectronics. *Chem. Rev.* **107**, 1011–1065 (2007).
207. Raza, E., Aziz, F. & Ahmad, Z. Stability of organometal halide perovskite solar cells and role of HTMs: recent developments and future directions. *RSC Adv.* **8**, 20952–20967 (2018).
208. Xu, B. et al. Efficient solid state dye-sensitized solar cells based on an oligomer hole transport material and an organic dye. *J. Mater. Chem. A Mater.* **1**, 14467 (2013).
209. Wang, S. et al. Role of 4-tert-butylpyridine as a hole transport layer morphological controller in perovskite solar cells. *Nano Lett.* **16**, 5594–5600 (2016).
210. Habisreutinger, S. N., Noel, N. K., Snaith, H. J. & Nicholas, R. J. Investigating the role of 4-tert butylpyridine in perovskite solar cells. *Adv. Energy Mater*. https://doi.org/10.1002/aenm.201601079 (2017).

211. Jena, A. K., Ikegami, M. & Miyasaka, T. Severe morphological deformation of spiro-OMeTAD in $(CH_3NH_3)PbI_3$ solar cells at high temperature. *ACS Energy Lett.* **2**, 1760–1761 (2017).
212. Lee, I., Yun, J. H., Son, H. J. & Kim, T.-S. Accelerated degradation due to weakened adhesion from Li-TFSI additives in perovskite solar cells. *ACS Appl. Mater. Interfaces* **9**, 7029–7035 (2017).
213. Malinauskas, T. et al. Enhancing thermal stability and lifetime of solid-state dye-sensitized solar cells via molecular engineering of the hole-transporting material spiro-OMeTAD. *ACS Appl. Mater. Interfaces* **7**, 11107–11116 (2015).
214. Zhao, X., Kim, H.-S., Seo, J.-Y. & Park, N.-G. Effect of selective contacts on the thermal stability of perovskite solar cells. *ACS Appl. Mater. Interfaces* **9**, 7148–7153 (2017).
215. Yue, Y. et al. Enhanced stability of perovskite solar cells through corrosion-free pyridine derivatives in hole-transporting materials. *Adv. Mater.* **28**, 10738–10743 (2016).
216. Jeon, I. et al. Single-walled carbon nanotube film as electrode in indium-free planar heterojunction perovskite solar cells: investigation of electron-blocking layers and dopants. *Nano Lett.* **15**, 6665–6671 (2015).
217. Nam, J.-S. et al. A facile and effective ozone exposure method for wettability and energy-level tuning of hole-transporting layers in lead-free tin perovskite solar cells. *ACS Appl. Mater. Interfaces* **13**, 42935–42943 (2021).
218. Kim, N. et al. Highly conductive PEDOT:PSS nanofibrils induced by solution-processed crystallization. *Adv. Mater.* **26**, 2268–2272 (2014).
219. Wang, M. et al. Defect passivation using ultrathin PTAA layers for efficient and stable perovskite solar cells with a high fill factor and eliminated hysteresis. *J. Mater. Chem. A Mater.* **7**, 26421–26428 (2019).
220. Chen, C. et al. Effect of BCP buffer layer on eliminating charge accumulation for high performance of inverted perovskite solar cells. *RSC Adv.* **7**, 35819–35826 (2017).
221. Shibayama, N., Kanda, H., Kim, T. W., Segawa, H. & Ito, S. Design of BCP buffer layer for inverted perovskite solar cells using ideal factor. *APL Mater.* **7**, 031117 (2019).
222. Zhang, X. et al. Improved fill factor in inverted planar perovskite solar cells with zirconium acetate as the hole-and-ion-blocking layer. *Phys. Chem. Chem. Phys.* **20**, 7395–7400 (2018).
223. Zhao, Z. Q. et al. Molecular modulator for stable inverted planar perovskite solar cells with efficiency enhanced by interface engineering. *J. Mater. Chem. C Mater.* **7**, 9735–9742 (2019).
224. Chen, L. et al. Improving the electrical performance of inverted perovskite solar cell with LiF anode buffer layer. *Org. Electron.* **101**, 106401 (2022).
225. Jeng, J. et al. $CH_3NH_3PbI_3$ perovskite/fullerene planar-heterojunction hybrid solar cells. *Adv. Mater.* **25**, 3727–3732 (2013).
226. Xiao, Z. et al. Efficient, high yield perovskite photovoltaic devices grown by interdiffusion of solution-processed precursor stacking layers. *Energy Environ. Sci.* **7**, 2619–2623 (2014).
227. Liang, P. et al. Additive enhanced crystallization of solution-processed perovskite for highly efficient planar-heterojunction solar cells. *Adv. Mater.* **26**, 3748–3754 (2014).
228. Xie, J. et al. A ternary organic electron transport layer for efficient and photostable perovskite solar cells under full spectrum illumination. *J. Mater. Chem. A Mater.* **6**, 5566–5573 (2018).
229. You, J. et al. Improved air stability of perovskite solar cells via solution-processed metal oxide transport layers. *Nat. Nanotechnol.* **11**, 75–81 (2016).
230. Liu, X. et al. Triple cathode buffer layers composed of PCBM, C60, and LiF for high-performance planar perovskite solar cells. *ACS Appl. Mater. Interfaces* **7**, 6230–6237 (2015).
231. Chang, C.-Y., Huang, W.-K., Chang, Y.-C., Lee, K.-T. & Chen, C.-T. A solution-processed n-doped fullerene cathode interfacial layer for efficient and stable large-area perovskite solar cells. *J. Mater. Chem. A Mater.* **4**, 640–648 (2016).
232. Wolff, C. M. et al. Reduced interface-mediated recombination for high open-circuit voltages in CH3NH3PbI3 solar cells. *Adv. Mater.* https://doi.org/10.1002/adma.201700159 (2017).
233. Lin, H.-S. et al. Achieving high efficiency in solution-processed perovskite solar cells using C60/C70 mixed fullerenes. *ACS Appl. Mater. Interfaces* **10**, 39590–39598 (2018).
234. Ueno, H. et al. Li@C60 endohedral fullerene as a supraatomic dopant for C60 electron-transporting layers promoting the efficiency of perovskite solar cells. *Chem. Commun.* **55**, 11837–11839 (2019).
235. Lee, C., Seo, Y., Han, J., Hwang, J. & Jeon, I. Perspectives on critical properties of fullerene derivatives for rechargeable battery applications. *Carbon* **210**, 118041 (2023).
236. Li, Y. et al. Multifunctional fullerene derivative for interface engineering in perovskite solar cells. *J. Am. Chem. Soc.* **137**, 15540–15547 (2015).
237. Zhang, M. et al. Reconfiguration of interfacial energy band structure for high-performance inverted structure perovskite solar cells. *Nat. Commun.* **10**, 4593 (2019).
238. Jia, L., Chen, M. & Yang, S. Functionalization of fullerene materials toward applications in perovskite solar cells. *Mater. Chem. Front.* **4**, 2256–2282 (2020).
239. Zhang, F. et al. Isomer-pure bis-PCBM-assisted crystal engineering of perovskite solar cells showing excellent efficiency and stability. *Adv. Mater.* https://doi.org/10.1002/adma.201606806 (2017).
240. Lin, H.-S. et al. Highly selective and scalable fullerene-cation-mediated synthesis accessing cyclo[60]fullerenes with five-membered carbon ring and their application to perovskite solar cells. *Chem. Mater.* **31**, 8432–8439 (2019).
241. Jeon, I. et al. Controlled redox of lithium-ion endohedral fullerene for efficient and stable metal electrode-free perovskite solar cells. *J. Am. Chem. Soc.* **141**, 16553–16558 (2019).
242. Jeon, I. et al. Lithium-ion endohedral fullerene (Li^+@C60) dopants in stable perovskite solar cells induce instant doping and anti-oxidation. *Angew. Chem. Int. Ed.* **57**, 4607–4611 (2018).
243. Mandler, D. & Kraus-Ophir, S. Self-assembled monolayers (SAMs) for electrochemical sensing. *J. Solid State Electrochem.* **15**, 1535–1558 (2011).
244. Gooding, J. J., Mearns, F., Yang, W. & Liu, J. Self-assembled monolayers into the 21st century: recent advances and applications. *Electroanalysis* **15**, 81–96 (2003).
245. Ulman, A. Formation and structure of self-assembled monolayers. *Chem. Rev.* **96**, 1533–1554 (1996).
246. Ali, F., Roldán-Carmona, C., Sohail, M. & Nazeeruddin, M. K. Applications of self-assembled monolayers for perovskite solar cells interface engineering to address efficiency and stability. *Adv. Energy Mater.* https://doi.org/10.1002/aenm.202002989 (2020).
247. Al-Ashouri, A. et al. Conformal monolayer contacts with lossless interfaces for perovskite single junction and monolithic tandem solar cells. *Energy Environ. Sci.* **12**, 3356–3369 (2019).
248. Yehye, W. A. et al. Understanding the chemistry behind the antioxidant activities of butylated hydroxytoluene (BHT): a review. *Eur. J. Med. Chem.* **101**, 295–312 (2015).
249. Reche-Tamayo, M., Moral, M., Pérez-Jiménez, A. J. & Sancho-García, J. C. Theoretical determination of interaction and cohesive energies of weakly bound cycloparaphenylene molecules. *J. Phys. Chem. C* **120**, 22627–22634 (2016).
250. Cacciuto, A., Auer, S. & Frenkel, D. Onset of heterogeneous crystal nucleation in colloidal suspensions. *Nature* **428**, 404–406 (2004).
251. Adil Afroz, M. et al. Thermal stability and performance enhancement of perovskite solar cells through oxalic acid-induced perovskite formation. *ACS Appl. Energy Mater.* **3**, 2432–2439 (2020).
252. Afroz, M. A., Garai, R., Gupta, R. K. & Iyer, P. K. Additive-assisted defect passivation for minimization of open-circuit voltage loss and improved perovskite solar cell performance. *ACS Appl. Energy Mater.* **4**, 10468–10476 (2021).
253. Borges, R. et al. Understanding the molecular aspects of tetrahydrocannabinol and cannabidiol as antioxidants. *Molecules* **18**, 12663–12674 (2013).
254. Kumar, S. et al. Multifaceted role of a dibutylhydroxytoluene processing additive in enhancing the efficiency and stability of planar perovskite solar cells. *ACS Appl. Mater. Interfaces* **11**, 38828–38837 (2019).
255. Liang, P., Chueh, C., Williams, S. T. & Jen, A. K.-Y. Roles of fullerene-based interlayers in enhancing the performance of organometal perovskite thin-film solar cells. *Adv. Energy Mater.* https://doi.org/10.1002/aenm.201402321 (2015).
256. Ruoff, R. S., Tse, D. S., Malhotra, R. & Lorents, D. C. Solubility of fullerene (C60) in a variety of solvents. *J. Phys. Chem.* **97**, 3379–3383 (1993).
257. Tajima, Y. et al. Surface free energy and wettability determination of various fullerene derivative films on amorphous carbon wafer. *Jpn. J. Appl. Phys.* **47**, 5730 (2008).
258. Kwiatkowski, J. J., Frost, J. M. & Nelson, J. The effect of morphology on electron field-effect mobility in disordered C60 thin films. *Nano Lett.* **9**, 1085–1090 (2009).
259. Akers, K. L., Douketis, C., Haslett, T. L. & Moskovits, M. Raman spectroscopy of C60 solid films: a tale of two spectra. *J. Phys. Chem.* **98**, 10824–10831 (1994).
260. Zang, Z., Nakamura, A. & Temmyo, J. Single cuprous oxide films synthesized by radical oxidation at low temperature for PV application. *Opt. Express* **21**, 11448 (2013).
261. Zang, Z., Nakamura, A. & Temmyo, J. Nitrogen doping in cuprous oxide films synthesized by radical oxidation at low temperature. *Mater. Lett.* **92**, 188–191 (2013).
262. Yoon, H., Kang, S. M., Lee, J.-K. & Choi, M. Hysteresis-free low-temperature-processed planar perovskite solar cells with 19.1% efficiency. *Energy Environ. Sci.* **9**, 2262–2266 (2016).
263. Ke, W. et al. Efficient planar perovskite solar cells using room-temperature vacuum-processed C60 electron selective layers. *J. Mater. Chem. A Mater.* **3**, 17971–17976 (2015).
264. Jeon, I. et al. Direct and dry deposited single-walled carbon nanotube films doped with MoO_x as electron-blocking transparent electrodes for flexible organic solar cells. *J. Am. Chem. Soc.* **137**, 7982–7985 (2015).
265. Jeon, I. et al. Carbon nanotubes versus graphene as flexible transparent electrodes in inverted perovskite solar cells. *J. Phys. Chem. Lett.* **8**, 5395–5401 (2017).
266. Jinno, H. et al. Stretchable and waterproof elastomer-coated organic photovoltaics for washable electronic textile applications. *Nat. Energy* **2**, 780–785 (2017).
267. Yoon, J. et al. Foldable perovskite solar cells using carbon nanotube-embedded ultrathin polyimide conductor. *Adv. Sci.* https://doi.org/10.1002/advs.202170033 (2021).
268. Lee, G. et al. Ultra-flexible perovskite solar cells with crumpling durability: toward a wearable power source. *Energy Environ. Sci.* **12**, 3182–3191 (2019).
269. Ongaro, C. et al. Integration of metal meshes as transparent conducting electrodes into perovskite solar cells. *Adv. Mater. Interfaces* https://doi.org/10.1002/admi.202300923 (2024).
270. De, S. et al. Silver nanowire networks as flexible, transparent, conducting films: extremely high DC to optical conductivity ratios. *ACS Nano* **3**, 1767–1774 (2009).
271. Lee, P. et al. Highly stretchable and highly conductive metal electrode by very long metal nanowire percolation network. *Adv. Mater.* **24**, 3326–3332 (2012).
272. Han, S. et al. Fast plasmonic laser nanowelding for a Cu-nanowire percolation network for flexible transparent conductors and stretchable electronics. *Adv. Mater.* **26**, 5808–5814 (2014).
273. Ravi Kumar, D. V., Woo, K. & Moon, J. Promising wet chemical strategies to synthesize Cu nanowires for emerging electronic applications. *Nanoscale* **7**, 17195–17210 (2015).
274. Critchley, K. et al. Near-bulk conductivity of gold nanowires as nanoscale interconnects and the role of atomically smooth interface. *Adv. Mater.* **22**, 2338–2342 (2010).
275. Kim, J., da Silva, W. J., bin Mohd Yusoff, Abd, R. & Jang, J. Organic devices based on nickel nanowires transparent electrode. *Sci. Rep.* **6**, 19813 (2016).

276. Li, Z. et al. Laminated carbon nanotube networks for metal electrode-free efficient perovskite solar cells. *ACS Nano* **8**, 6797–6804 (2014).
To our knowledge, this article reports the first carbon nanotube-based, metal-electrode-free perovskite solar cell.
277. Yoon, J. et al. Superflexible, high-efficiency perovskite solar cells utilizing graphene electrodes: towards future foldable power sources. *Energy Environ. Sci.* **10**, 337–345 (2017).
278. Jeon, I. et al. Perovskite solar cells using carbon nanotubes both as cathode and as anode. *J. Phys. Chem. C* **121**, 25743–25749 (2017).
279. Jeon, I., Xiang, R., Shawky, A., Matsuo, Y. & Maruyama, S. Single-walled carbon nanotubes in emerging solar cells: synthesis and electrode applications. *Adv. Energy Mater.* **9**, 1801312 (2019).
280. Choi, J. et al. Overview and outlook on graphene and carbon nanotubes in perovskite photovoltaics from single-junction to tandem applications. *Adv. Funct. Mater*. https://doi.org/10.1002/adfm.202204594 (2022).
This review provides an overview of all nanocarbon-based perovskite solar cells.
281. Huang, Y. et al. Nanoelectronic biosensors based on CVD grown graphene. *Nanoscale* **2**, 1485 (2010).
282. Utsumi, S. et al. Giant nanomechanical energy storage capacity in twisted single-walled carbon nanotube ropes. *Nat. Nanotechnol.* **19**, 1007–1015 (2024).
283. Zhang, Q. et al. Large-diameter carbon nanotube transparent conductor overcoming performance–yield tradeoff. *Adv. Funct. Mater*. https://doi.org/10.1002/adfm.202103397 (2022).
284. Kim, U. et al. Enhanced performance of solution-processed carbon nanotube transparent electrodes in foldable perovskite solar cells through vertical separation of binders by using eco-friendly parylene substrate. *Carbon Energy* https://doi.org/10.1002/cey2.471 (2024).
285. Shawky, A. et al. Controlled removal of surfactants from double-walled carbon nanotubes for stronger p-doping effect and its demonstration in perovskite solar cells. *Small Methods* **5**, e2100080 (2021).
286. Jeon, I. et al. High-performance solution-processed double-walled carbon nanotube transparent electrode for perovskite solar cells. *Adv. Energy Mater.* **9**, 1901204 (2019).
287. Yu, L., Shearer, C. & Shapter, J. Recent development of carbon nanotube transparent conductive films. *Chem. Rev.* **116**, 13413–13453 (2016).
288. Zhang, Q., Wei, N., Laiho, P. & Kauppinen, E. I. Recent developments in single-walled carbon nanotube thin films fabricated by dry floating catalyst chemical vapor deposition. *Top. Curr. Chem.* **375**, 90 (2017).
289. Sun, L. et al. All-solution-processed ultraflexible wearable sensor enabled with universal trilayer structure for organic optoelectronic devices. *Sci. Adv.* **10**, eadk9460 (2024).
290. Kim, J. et al. Liquid metal-based perovskite solar cells: in situ formed gallium oxide interlayer improves stability and efficiency. *Adv. Funct. Mater*. https://doi.org/10.1002/adfm.202311597 (2024).
291. Mahmood, K. et al. Solution processed high performance perovskite solar cells based on a silver nanowire-titanium dioxide hybrid top electrode. *RSC Adv.* **12**, 35350–35357 (2022).
292. Han, K. et al. Fully solution processed semi-transparent perovskite solar cells with spray-coated silver nanowires/ZnO composite top electrode. *Sol. Energy Mater. Sol. Cell* **185**, 399–405 (2018).
293. Jeon, I. et al. Carbon nanotubes to outperform metal electrodes in perovskite solar cells via dopant engineering and hole-selectivity enhancement. *J. Mater. Chem. A Mater.* **8**, 11141–11147 (2020).
To our knowledge, this article reports the first instance of carbon nanotube electrodes outperforming metal electrodes in perovskite solar cells.
294. Seo, S. et al. Multi-functional MoO_3 doping of carbon-nanotube top electrodes for highly transparent and efficient semi-transparent perovskite solar cells. *Adv. Mater. Interfaces* **9**, 2101595 (2022).
295. Fagiolari, L. & Bella, F. Carbon-based materials for stable, cheaper and large-scale processable perovskite solar cells. *Energy Environ. Sci.* **12**, 3437–3472 (2019).
296. Bogachuk, D. et al. Low-temperature carbon-based electrodes in perovskite solar cells. *Energy Environ. Sci.* **13**, 3880–3916 (2020).
297. Lee, C. et al. Carbon nanotube electrode-based perovskite–silicon tandem solar cells. *Solar RRL* **4**, 2000353 (2020).
298. Lee, J., Menamparambath, M. M., Hwang, J. & Baik, S. Hierarchically structured hole transport layers of spiro-OMeTAD and multiwalled carbon nanotubes for perovskite solar cells. *ChemSusChem* **8**, 2358–2362 (2015).
299. Zheng, X. et al. Boron doping of multiwalled carbon nanotubes significantly enhances hole extraction in carbon-based perovskite solar cells. *Nano Lett.* **17**, 2496–2505 (2017).
300. Yu, Y., Hoang, M. T., Yang, Y. & Wang, H. Critical assessment of carbon pastes for carbon electrode-based perovskite solar cells. *Carbon* **205**, 270–293 (2023).
301. Wagner, L., Mastroianni, S. & Hinsch, A. Reverse manufacturing enables perovskite photovoltaics to reach the carbon footprint limit of a glass substrate. *Joule* **4**, 882–901 (2020).
302. Xiao, C. et al. Mechanisms of electron-beam-induced damage in perovskite thin films revealed by cathodoluminescence spectroscopy. *J. Phys. Chem. C* **119**, 26904–26911 (2015).
303. Lee, J.-H. & Lee, J.-W. van der Waals metal contacts for characterization and optoelectronic application of metal halide perovskite thin films. *ACS Energy Lett.* **7**, 3780–3787 (2022).
304. Paek, S. et al. Dopant-free hole-transporting materials for stable and efficient perovskite solar cells. *Adv. Mater*. https://doi.org/10.1002/adma.201606555 (2017).
305. Unger, E. L. et al. Hysteresis and transient behavior in current–voltage measurements of hybrid-perovskite absorber solar cells. *Energy Environ. Sci.* **7**, 3690–3698 (2014).
306. Wang, Y. et al. Reliable measurement of perovskite solar cells. *Adv. Mater*. https://doi.org/10.1002/adma.201803231 (2019).
307. Tang, H. et al. Interface engineering for highly efficient organic solar cells. *Adv. Mater.* **36**, e2212236 (2024).
308. Xiao, Y., Yang, X., Zhu, R. & Snaith, H. J. Unlocking interfaces in photovoltaics. *Science* **384**, 846–848 (2024).
309. Dong, Q. et al. Interpenetrating interfaces for efficient perovskite solar cells with high operational stability and mechanical robustness. *Nat. Commun.* **12**, 973 (2021).
310. Yang, S., Fu, W., Zhang, Z., Chen, H. & Li, C.-Z. Recent advances in perovskite solar cells: efficiency, stability and lead-free perovskite. *J. Mater. Chem. A Mater.* **5**, 11462–11482 (2017).
311. Li, Y. et al. High-efficiency robust perovskite solar cells on ultrathin flexible substrates. *Nat. Commun.* **7**, 10214 (2016).
312. Bush, K. A. et al. 23.6%-efficient monolithic perovskite/silicon tandem solar cells with improved stability. *Nat. Energy* **2**, 17009 (2017).
313. Romano, V., Agresti, A., Verduci, R. & D'Angelo, G. Advances in perovskites for photovoltaic applications in space. *ACS Energy Lett.* **7**, 2490–2514 (2022).
314. Tu, Y. et al. Perovskite solar cells for space applications: progress and challenges. *Adv. Mater.* **33**, 2006545 (2021).
315. Aydin, E. et al. Pathways toward commercial perovskite/silicon tandem photovoltaics. *Science* **383**, eadh3849 (2024).
316. Mariotti, S. et al. Interface engineering for high-performance, triple-halide perovskite–silicon tandem solar cells. *Science* **381**, 63–69 (2023).
317. Chin, X. Y. et al. Interface passivation for 31.25%-efficient perovskite/silicon tandem solar cells. *Science* **381**, 59–63 (2023).
318. Shi, Y., Berry, J. J. & Zhang, F. Perovskite/silicon tandem solar cells: insights and outlooks. *ACS Energy Lett.* **9**, 1305–1330 (2024).
319. Yuan, Y. & Huang, J. Ion migration in organometal trihalide perovskite and its impact on photovoltaic efficiency and stability. *Acc. Chem. Res.* **49**, 286–293 (2016).
320. Calado, P. et al. Evidence for ion migration in hybrid perovskite solar cells with minimal hysteresis. *Nat. Commun.* **7**, 13831 (2016).
321. Lee, J.-W., Kim, S.-G., Yang, J.-M., Yang, Y. & Park, N.-G. Verification and mitigation of ion migration in perovskite solar cells. *APL Mater.* **7**, 41111 (2019).
322. Yoon, S. J. et al. Tracking iodide and bromide ion segregation in mixed halide lead perovskites during photoirradiation. *ACS Energy Lett.* **1**, 290–296 (2016).
323. Knight, A. J. et al. Electronic traps and phase segregation in lead mixed-halide perovskite. *ACS Energy Lett.* **4**, 75–84 (2019).
324. Leijtens, T., Bush, K. A., Prasanna, R. & McGehee, M. D. Opportunities and challenges for tandem solar cells using metal halide perovskite semiconductors. *Nat. Energy* **3**, 828–838 (2018).
325. Liu, K. et al. Reducing sputter induced stress and damage for efficient perovskite/silicon tandem solar cells. *J. Mater. Chem. A Mater.* **10**, 1343–1349 (2022).
326. Liu, K., Wang, Z., Qu, S. & Ding, L. Stress and strain in perovskite/silicon tandem solar cells. *Nanomicro Lett.* **15**, 59 (2023).
327. Holzhey, P. & Saliba, M. A full overview of international standards assessing the long-term stability of perovskite solar cells. *J. Mater. Chem. A Mater.* **6**, 21794–21808 (2018).
328. Duan, L. et al. Stability challenges for the commercialization of perovskite–silicon tandem solar cells. *Nat. Rev. Mater.* **8**, 261–281 (2023).
329. Repins, I. L., Kersten, F., Hallam, B., VanSant, K. & Koentopp, M. B. Stabilization of light-induced effects in Si modules for IEC 61215 design qualification. *Sol. Energy* **208**, 894–904 (2020).
330. Rosenthal, A. L., Thomas, M. G. & Durand, S. J. A ten year review of performance of photovoltaic systems. In *Conference Record of the Twenty Third IEEE Photovoltaic Specialists Conf. — (Cat. No. 93CH3283-9)* 1289–1291 (IEEE, 1993).
331. Domanski, K., Alharbi, E. A., Hagfeldt, A., Grätzel, M. & Tress, W. Systematic investigation of the impact of operation conditions on the degradation behaviour of perovskite solar cells. *Nat. Energy* **3**, 61–67 (2018).
332. Saliba, M., Stolterfoht, M., Wolff, C. M., Neher, D. & Abate, A. Measuring aging stability of perovskite solar cells. *Joule* **2**, 1019–1024 (2018).
333. Wu, S. et al. A chemically inert bismuth interlayer enhances long-term stability of inverted perovskite solar cells. *Nat. Commun.* **10**, 1161 (2019).
334. Perovskite Solar Cell Market Size, Share & Trends Analysis Report By Product (Flexible, Rigid), By Vertical, By Application (Smart Glass, BIPV, Solar Panel), By Region, And Segment Forecasts, 2024 - 2030. *Grand View Research* https://www.grandviewresearch.com/industry-analysis/perovskite-solar-cell-market-report (2024).
335. John, R. A. et al. Reconfigurable halide perovskite nanocrystal memristors for neuromorphic computing. *Nat. Commun.* **13**, 2074 (2022).
336. Nam, J. et al. Enhanced photodetection and air stability of lead-free tin perovskite photodiodes via germanium incorporation and organic cation-mediated dimensionality control. *Adv. Funct. Mater*. https://doi.org/10.1002/adfm.202407299 (2024).
337. Sakhatskyi, K. et al. Stable perovskite single-crystal X-ray imaging detectors with single-photon sensitivity. *Nat. Photon.* **17**, 510–517 (2023).
338. Tian, X., Stranks, S. D. & You, F. Life cycle energy use and environmental implications of high-performance perovskite tandem solar cells. *Sci. Adv.* **6**, eabb0055 (2020).
339. Kadro, J. M. & Hagfeldt, A. The end-of-life of perovskite PV. *Joule* **1**, 634 (2017).
340. Hailegnaw, B., Kirmayer, S., Edri, E., Hodes, G. & Cahen, D. Rain on methylammonium lead iodide based perovskites: possible environmental effects of perovskite solar cells. *J. Phys. Chem. Lett.* **6**, 1543–1547 (2015).

341. Vidal, R. et al. Assessing health and environmental impacts of solvents for producing perovskite solar cells. *Nat. Sustain.* **4**, 277–285 (2020).
342. Kim, H. J., Han, G. S. & Jung, H. S. Managing the lifecycle of perovskite solar cells: addressing stability and environmental concerns from utilization to end-of-life. *eScience* **4**, 100243 (2024).
343. Rosales, B. A., Schutt, K., Berry, J. J. & Wheeler, L. M. Leveraging low-energy structural thermodynamics in halide perovskites. *ACS Energy Lett.* **8**, 1705–1715 (2023).
344. Zhang, J. et al. Optimizing perovskite thin-film parameter spaces with machine learning-guided robotic platform for high-performance perovskite solar cells. *Adv. Energy Mater*. https://doi.org/10.1002/aenm.202302594 (2023).
345. Xu, Z. et al. Advancing perovskite solar cell commercialization: bridging materials, vacuum deposition, and AI-assisted automation. *Next Mater.* **3**, 100103 (2024).
346. Wang, R. et al. A review of perovskites solar cell stability. *Adv. Funct. Mater*. https://doi.org/10.1002/adfm.201808843 (2019).

Acknowledgements

J.H., K.P. and S.T contributed equally to this study. J.H. and I.J. acknowledge support from the National Research Foundation of Korea (NRF) grant funded by the Korea government (MSIT) under numbers 2023R1A2C3007358, RS-2023-00228994, RS-2023-00243849 and RS-2024-00459908. J.-W.L. acknowledges support from an NRF grant funded by the Korean government (Ministry of Science and ICT) under contract numbers 2022R1C1C1011975 and 2022M3J1A1064315. S.T. was supported by the US Department of Energy's Office of Energy Efficiency and Renewable Energy (EERE) under the Solar Energy Technologies Office under award number DE-EE0010503. Large Language Models (LLMs), namely, ChatGPT 4o and Claude 3.5 Sonnet, were used for copyediting purposes. This project has received funding from the European Research Council (ERC) under the European Union's Horizon 2020 research and innovation programme (ERC Grant Agreement no. 101087679, PEROVAP) and the Deutsche Forschungsgemeinschaft (DFG) in the framework of the Special Priority Program (SPP 2196) project PERFECT PVs (no. 424216076).

Author contributions

Introduction (J.-W.L. and I.J.); Experimentation (J.H., K.P., S.T., Y.V., J.X., E.W.-G.D., M.G.B., J.-W.L. and I.J.); Results (J.H., K.P., S.T., Y.V., J.X., E.W.-G.D., M.G.B., J.-W.L. and I.J.); Applications (J.H., K.P., J.-W.L. and I.J.); Reproducibility and data deposition (J.H., K.P., S.T., J.-W.L. and I.J.); Limitations and optimizations (J.H., K.P., S.T., J.-W.L. and I.J.); Outlook (M.G.B., J.-W.L. and I.J.); overview of the Primer (all authors).

Competing interests

The authors declare no competing interests.

Additional information

Peer review information *Nature Reviews Methods Primers* thanks Yi Hou, Antonio Abate and the other, anonymous, reviewer(s) for their contribution to the peer review of this work.

Related links

National Renewable Energy Laboratory: https://www.nrel.gov/pv/cell-efficiency.html